Zero-G Class Underwater Robots: Unrestricted Attitude Control Using Control Moment Gyros

Blair Thornton, *Member, IEEE*, Tamaki Ura, *Fellow, IEEE*, Yoshiaki Nose, and Stephen Turnock

***Abstract*—The "Zero-G" is designated as a new class of underwater robot that is capable of unrestricted attitude control. A novel control scheme based on internal actuation using control moment gyros (CMGs) is developed to provide Zero-G class autonomous underwater vehicles (AUVs) with this unique freedom in control. This is implemented in the CMG-actuated Zero-G class internal kinematic underwater robot actuation (IKURA) system that was developed as part of this research. A series of experiments are performed to demonstrate the practical application of CMGs and verify the associated theoretical developments. The ability to actively stabilize the translational dynamics of the robot is assessed and unrestricted attitude control is demonstrated in an experiment that involves vertically pitched diving and surfacing in surge. Finally, potential applications for Zero-G class AUVs are discussed.**

***Index Terms*—Control moment gyro (CMG), internal kinematic underwater robot actuation (IKURA), internal actuation, underwater robot, unrestricted attitude control, Zero-G.**

I. Introduction

THE ocean is a vast 3-D environment and it follows that an ocean research tool, such as the autonomous underwater vehicle (AUV), should ideally be able to move freely in any direction within its surroundings. The ability to adopt and maintain any attitude on the surface of a sphere with a zero radius turning circle would allow an intelligent underwater robot to approach its missions in a fully 3-D manner, optimizing the use of its thrusters, sensors, and power supply in a way that has not been possible previously. It is thought that, in addition to improving AUV performance, unrestricted attitude control will open up new fields of research where AUVs can be applied. It is further thought that internal actuation techniques can provide this freedom in control. The aim of this research is to develop a new class of "Zero-G" AUV that is capable of unrestricted attitude control. This unique freedom in control is achieved through the pursuit of the following two complementary goals:

Manuscript received December 23, 2005; revised October 16, 2006; accepted February 28, 2007. This work was supported by the Monbukagakusho, Japanese Ministry of Education under the advanced research scholarship.

Associate Editor: D. R. Blidberg.

B. Thornton was with the School of Engineering Science, University of Southampton, Southampton SO17 1BJ, U.K. He is now with the Underwater Robotics and Application (URA) Laboratory, University of Tokyo, Tokyo 153-8505, Japan (e-mail: blair@iis.u-tokyo.ac.jp).

T. Ura and Y. Nose are with the Underwater Robotics and Application (URA) Laboratory, University of Tokyo, Tokyo 153-8505, Japan (e-mail: ura@iis.u-tokyo.ac.jp; ynose@iis.u-tokyo.ac.jp).

S. Turnock is with the School of Engineering Science, University of Southampton, Southampton SO17 1BJ, U.K. (e-mail: steve@ship.soton.ac.uk).

Color versions of one or more of the figures in this paper are available online at http://ieeexplore.ieee.org.

Digital Object Identifier 10.1109/JOE.2007.899274

- the introduction of control moment gyros (CMGs) as a new type of underwater actuator;
- the development of a novel unrestricted attitude control scheme, for a body with zero righting moment, based on internal momentum exchange using CMGs.

The last 25 years have seen AUVs evolve into two main classes. The most widely seen is the "cruising" class that performs various large area observations [1]–[3]. These robots have lengths in the order of 4 to 10 m and operate at a safe distance from their target, travelling predominantly in surge using a main thruster supplemented by fins and rudders for directional control. The demand for robots to operate closer to their targets and carry out detailed inspection, mapping, and even manipulation tasks has seen the development of smaller and more agile "hovering" class AUVs [4]–[6]. These typically have lengths between 1.5 and 2 m and operate at low speeds using multiple thrusters for independent control over several degrees of freedom so that they can cope with sudden changes in the geometry of the target. Underwater robotics is a diverse field and the various applications demand a number of different types of AUV in addition to the traditional main classes. Underwater gliders are extremely efficient in terms of power consumption and are capable of travelling long distances by varying their buoyancy, using foils to deflect fluid momentum and propel themselves through the open ocean [7], [8]. Other alternatives include biomimetic AUVs that draw inspiration from the actuation techniques of marine creatures [9], [10]. These often have articulated or flexible bodies that undulate and generate hydrodynamic forces to propel themselves through the water. To date, however, untethered underwater robots have relied on passive stability to maintain a usable orientation, applying limited or in some cases no active control about the roll and pitch axes. This confines their motion to that along a series of 2-D planes through the water and thereby limits their applications.

This research introduces the Zero-G as a new class of underwater robot that is capable of approaching its missions in a truly 3-D manner. This is defined as any underwater robot that can do the following:

- adopt and maintain any attitude on the surface of a sphere with a zero radius turning circle;
- actively stabilize any attitude while translating in surge.

To satisfy the first point, the robot should ideally have coincident centers of gravity and buoyancy and thus zero righting moment so that it can maneuver as if in a zero gravity environment. However, this freedom in control comes at the cost of stability in roll and pitch. Therefore, the attitude control system must actively stabilize the necessary fast angular rotations about these axes as well as achieve the desired orientation. This requires

a closed-loop attitude control system that can manage any orientation to provide independent control over all three rotational axes with a zero radius turning circle. The second point requires a single propulsion unit to actuate surge. This is not restrictive as the freedom in attitude control allows Zero-G class underwater robots to maneuver freely in any direction and approach their missions in a fully 3-D manner while travelling only in their principal mode of translation. Beyond the aforementioned specification, Zero-G class underwater robots should be considerably smaller than most existing AUVs, with lengths in the order of 0.5 m. The primary reason for this is to allow missions to be carried out in geometrically complicated, cluttered, and even enclosed environments. A small size not only allows for greater agility, but also allows the robot to maneuver in confined spaces.

The actuation and control requirements of Zero-G class underwater robots, in particular concerning the rotational dynamics, are very different to those of existing classes of AUV, demanding a speed and resolution of control that lies beyond the operational envelope of traditional underwater actuators. Actuators that deflect fluid momentum, such as fins and rudders, lose control authority at low velocities. Although actuators that generate fluid momentum, such as thrusters, can provide low-velocity control, the use of multiple thrusters increases drag, reducing efficiency particularly when travelling at high speeds. The inherent limitations of conventional actuators lead one to consider alternative means of actuation. Internal actuation devices present many advantages over traditional underwater actuators. Since they are contained within the body of the robot, they preserve the hydrodynamic integrity of its hull. Furthermore, they are protected from the harsh underwater environment and do not exert any external forces, which is of practical benefit when operating in proximity to loose surfaces or small creatures. In contrast to thrusters and fins that rely on relative fluid motion, internal actuators generate their own momentum and apply their control to the robot directly. Therefore, their performance is independent of external conditions and their control authority is maintained over the entire operating envelope, including low speed and even stationary conditions. This offers a speed and resolution of response that extends beyond that which can be achieved using traditional underwater actuation methods. Such devices present their greatest advantage when used to complement traditional actuators, in particular, the use of internal torque generators for attitude control greatly reduces the required number of thrusters and allows for simple and elegant design. It is contended that the control response offered by internal actuation techniques, specifically CMGs, opens a path to develop sophisticated Zero-G class underwater robots and their application to new fields of underwater research.

The use of internal momentum exchange devices to control underwater vehicles was first suggested by Leonard [11] in 1998, and has been the subject of ongoing research leading to the development of the internally actuated modular bodied untethered submersible (IAMBUS) [12] in 2003 that uses momentum wheels to control its attitude. CMGs generate larger torques than equivalent momentum wheels and have been the subject of much research starting in 1966 [13]. Since then, CMG systems have found practical applications in space, most notably in the Russian space station MIR [14]. However, despite their application for attitude control of space vehicles, CMGs have not previously been applied to underwater robots.

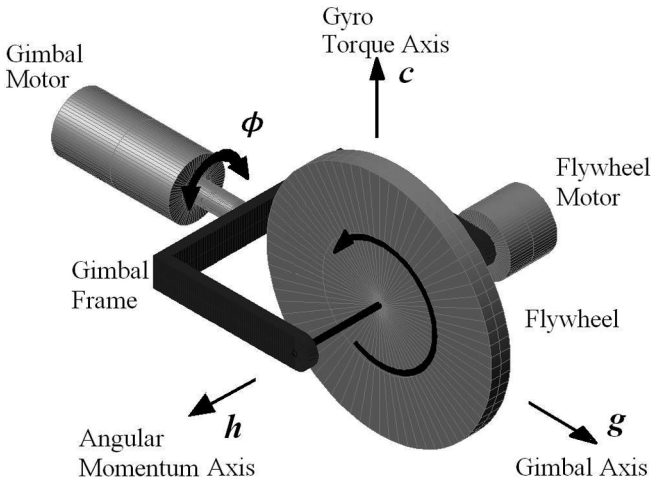

Fig. 1. Single gimbal CMG unit: Rotations of the gimbal change the flywheel's angular momentum vector and through internal momentum exchange a gyroscopic torque is generated that is used to actuate the robot.

II. Problem Formulation

A single gimbal CMG is a torque generator that consists of a flywheel mounted orthogonally on an actuated gimbal, as illustrated in Fig. 1.

A schematic for three-axis attitude control using CMGs is shown in Fig. 2. The main feature is that, in addition to the primary control law, a separate steering law is required to overcome the singularity problem of CMGs. This paper describes both theoretical and practical developments to realize such a system. The theoretical steps necessary are as follows:

- derivation of a fully descriptive model for the dynamics of the system in any orientation;
- formulation of a three-axis attitude control law that is suitable for application to AUVs;
- analysis of the singularities and null motion of CMGs to develop a mathematical escapability condition;
- formulation of a steering law that exactly achieves the desired torques while guaranteeing real-time singularity avoidance.

Beyond the aforementioned problem formulation, the practical application of the control system is assessed using the CMG-actuated, Zero-G class internal kinematic underwater robot actuation (IKURA) system. This is an experimental platform developed as part of this research to verify the theoretical developments and to demonstrate unrestricted attitude control. Finally, potential applications of Zero-G class AUVs are discussed.

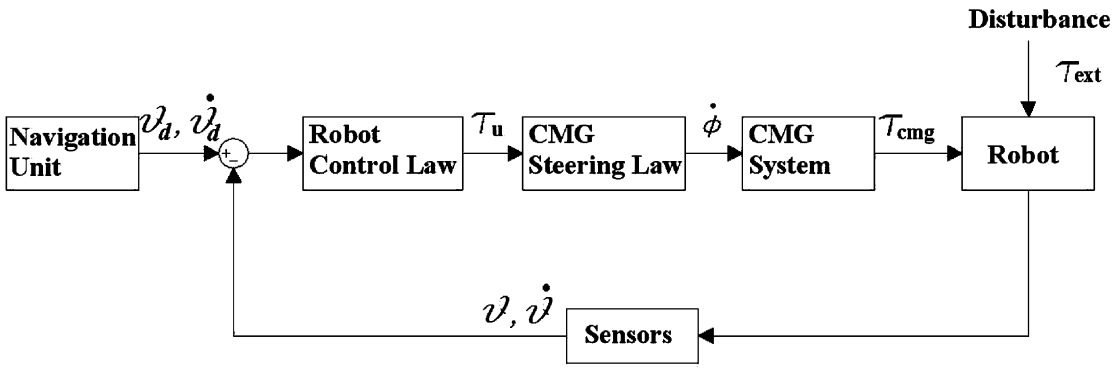

Fig. 2. Three-axis attitude control using CMGs: The navigation unit determines the desired state to complete a mission. The control law determines the torque required to achieve this state. The steering law computes the required CMG motion to produce this command torque.

III. System Equations of Motion

A. CMG Dynamics

A CMG system is composed of a number of identical CMG units arranged in a defined configuration. For each unit, the flywheel spins with an angular momentum vector along its axis of rotation h_i. For single gimbal units, the state of the system is defined by the angle ϕ_i about the gimbal axis g_i, which is orthogonal to the momentum axis. Rotations of the gimbal generate a gyroscopic torque that acts about the mutually orthogonal axis c_i and has a magnitude equal to the vector rate of change of the angular momentum stored. The unit vectors form a rotating coordinate system that tracks the nutation and precession of each CMG to follow its orientation. The relationship of the vectors is described by

$$c_i = \frac{\partial h_i}{\partial \phi_i} = h_i \times g_i. \tag{1}$$

The gimbal axis g_i is fixed and the momentum and torque axes h_i and c_i vary as functions of the gimbal angle

$$h_i = h_{i0}\cos\phi_i - c_{i0}\sin\phi_i$$
$$c_i = c_{i0}\cos\phi_i + h_{i0}\sin\phi_i$$

where h_{i0} and c_{i0} are the nominal states of the system.

Consider now the case of N identical CMG units in some fixed configuration. The orientation of each unit is defined by the vector of gimbal angles $\bar{\phi} = [\phi_1, \phi_2, \ldots, \phi_N]^T$, which defines the CMG state and specifies the $[3 \times N]$ gimbal, momentum and torque matrices $\bar{g}$, $\bar{h}$, and $\bar{c}$. The time derivatives of $\bar{h}$ and $\bar{c}$ vary as functions of the gimbal rates

$$\dot{\bar{h}} = -\bar{c}\,\mathrm{diag}(\dot{\bar{\phi}})$$
$$\dot{\bar{c}} = \bar{h}\,\mathrm{diag}(\dot{\bar{\phi}}). \tag{2}$$

The energy of the system can be expressed in matrix form

$$\mathbf{T}_{\mathrm{cmg}} = \frac{1}{2}\boldsymbol{\Omega}^T \mathbf{J}_{\mathrm{cmg}} \boldsymbol{\Omega}$$

where $\mathbf{J}_{\mathrm{cmg}}$ is the inertia of the CMGs and $\boldsymbol{\Omega}$ describes their rotational motion. For single gimbal systems, $\bar{g}$ is constant and so the motion of the CMG system can be described by the angular rate matrix

$$\boldsymbol{\Omega} = \bar{g}\dot{\bar{\phi}} + \bar{h}\dot{\bar{\psi}}$$

where $\dot{\bar{\psi}}$ is the angular velocity of each flywheel. The inertia varies as the gimbals rotate and can be expressed as

$$\mathbf{J}_{\mathrm{cmg}} = \bar{c}\mathbf{J}_c\bar{c}^T + \bar{g}\mathbf{J}_g\bar{g}^T + \bar{h}\mathbf{J}_h\bar{h}^T.$$

Noting that the gimbal axes themselves are fixed, the derivative $\mathbf{J}_{\mathrm{cmg}}$ can be obtained using the relationship (2)

$$\dot{\mathbf{J}}_{\mathrm{cmg}} = \mathrm{diag}\,\dot{\bar{\phi}}\bar{h}(\mathbf{J}_c - \mathbf{J}_h)\bar{c}^T + \mathrm{diag}\,\dot{\bar{\phi}}\bar{c}(\mathbf{J}_c - \mathbf{J}_h)\bar{h}^T$$

which can be expressed as a function of the gimbal rates

$$\dot{\mathbf{J}}_{\mathrm{cmg}} = \left[\left(h_1c_1^T + c_1h_1^T\right)\ldots\left(h_Nc_N^T + c_Nh_N^T\right)\right](\mathbf{J}_c - \mathbf{J}_h)\dot{\bar{\phi}}. \tag{3}$$

The angular momentum of the CMG system can be obtained by taking the derivative of the energy $\mathbf{T}_{\mathrm{cmg}}$ with respect to $\boldsymbol{\Omega}$, as follows:

$$\mathbf{h}_{\mathrm{cmg}} = \frac{\partial \mathbf{T}}{\partial \boldsymbol{\Omega}} = \bar{g}\mathbf{J}_g\dot{\bar{\phi}} + \bar{h}\mathbf{J}_h\dot{\bar{\psi}}.$$

Noting that the flywheels have a constant velocity, the torque of the CMG system can be expressed as a function of the gimbal rates by taking the time derivative of the angular momentum and substituting in (2)

$$\tau_{\mathrm{cmg}} = \bar{g}\mathbf{J}_g\ddot{\bar{\phi}} - \bar{c}\,\mathrm{diag}(\mathbf{J}_h\dot{\bar{\psi}})\dot{\bar{\phi}}. \tag{4}$$

The first term describes the torque inputs required to rotate the gimbals and the second term describes the gyroscopic outputs generated. The output is a function of the momentum stored in the flywheels and so large gains can be achieved. Furthermore, no component of the output acts in the flywheel or gimbal directions and so this setup is capable of a fast response to changes in input.

B. Coupled Dynamics

Consider a rigid body in which a system of N CMGs is placed. The total inertia of the system can be expressed as

$$\mathbf{J}_{\text{tot}} = \mathbf{J}_s + \mathbf{J}_{\text{cmg}}$$

where $\mathbf{J}_s$ is the inertia of the rigid body. The inertia of the CMG system varies with respect to the body-fixed reference frame $\mathbf{F_b}$, with its axes (x, y, z) aligned with the principal axes of the body. The body is free to translate and rotate with respect to the inertially fixed reference frame $\mathbf{F_i}$, with the axes (i, j, k). The coordinate system is illustrated in Fig. 3. In contrast to previous CMG applications that consider a stationary body in space, this application considers a body moving through a viscous fluid and so the effects of translational motion and any hydrodynamic interactions must be accounted for. The equations of motion of the system are derived using Kirchhoff's equations based on the dynamic energy of the complete CMG, body, and fluid system. These provide a dynamic model of a neutrally buoyant rigid body translating and rotating in an infinite volume of fluid. The fluid is assumed to be irrotational, incompressible, inviscid, and at rest at an infinitely distant boundary. While these assumptions initially seem restrictive, the equations can accommodate viscous effects, and any other unaccounted inputs, by appending them as external forces and moments. Kirchhoff's equations relate the dynamic energy of the system to the forces and moments that act on it

$$\begin{aligned} \frac{d}{dt}\left(\frac{\partial \mathbf{T}}{\partial u}\right) + \omega \times \left(\frac{\partial \mathbf{T}}{\partial u}\right) &= F_{\text{ext}} \\ \frac{d}{dt}\left(\frac{\partial \mathbf{T}}{\partial \omega}\right) + \omega \times \left(\frac{\partial \mathbf{T}}{\partial \omega}\right) + u \times \left(\frac{\partial T}{\partial u}\right) &= \tau_{\text{ext}} \end{aligned} \tag{5}$$

where u and ω are the translational and rotational velocity components of the body (Fig. 3). The kinetic energy of a submerged body consists of both solid and fluid components. The solid component is composed of the rigid body and CMG energy, and can be described as

$$\mathbf{T}_s = \frac{1}{2}\begin{pmatrix} u \\ \omega \\ \mathbf{\Omega} \end{pmatrix}^T \begin{pmatrix} m\mathbf{I} & 0 & 0 \\ 0 & \mathbf{J}_{\text{tot}} & \mathbf{J}_{\text{cmg}} \\ 0 & \mathbf{J}_{\text{cmg}} & \mathbf{J}_{\text{cmg}} \end{pmatrix} \begin{pmatrix} u \\ \omega \\ \mathbf{\Omega} \end{pmatrix}$$

where m is the total mass of the rigid body and the CMGs. The discussion is restricted to a body with coincident centers of gravity and buoyancy as this concept is central to the development of underwater robots with unrestricted attitude control capabilities. The fluid energy component can be expressed as

$$\mathbf{T}_l = \frac{1}{2}\begin{pmatrix} u \\ \omega \\ \mathbf{\Omega} \end{pmatrix}^T \begin{pmatrix} \mathbf{M}_A & \mathbf{D}_A & 0 \\ \mathbf{D}_A & \mathbf{J}_A & 0 \\ 0 & 0 & 0 \end{pmatrix} \begin{pmatrix} u \\ \omega \\ \mathbf{\Omega} \end{pmatrix}$$

where $\mathbf{M}_A$, $\mathbf{J}_A$, and $\mathbf{D}_A$ are the added mass, inertia, and inertial coupling matrices associated with the potential flow. These terms depend on the external shape of the body and the choice of coordinate frame. The dynamics of the system are greatly simplified by choosing a body with three planes of symmetry

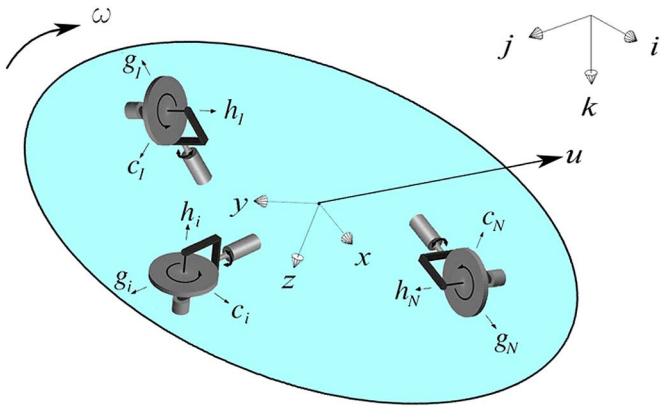

Fig. 3. Coordinate system: The cluster of N CMG units is fixed in a rigid body with the axes (x, y, z) that is free to translate and rotate with respect to the inertially fixed reference frame with the axes (i, j, k).

with the body coordinate frame along its principal axes as this reduces $\mathbf{M}_A$ and $\mathbf{J}_A$ to diagonal matrices and $\mathbf{D}_A$ to zero, and thus, fluid energy becomes uncoupled between the different degrees of freedom. The CMGs themselves make no contribution to the fluid energy since they are completely isolated from the external environment. The linear and angular momentum of the system can be obtained by taking the partial derivatives of the total energy with respect to u and ω

$$\mathbf{P} = \frac{\partial \mathbf{T}}{\partial u} = (m\mathbf{I} + \mathbf{M}_A)u \tag{6}$$

$$\mathbf{\Pi} = \frac{\partial \mathbf{T}}{\partial \omega} = (\mathbf{J}_{\text{tot}} + \mathbf{J}_A)\omega + \mathbf{h}_{\text{cmg}}. \tag{7}$$

Noting that the rigid body component of $\mathbf{J}_{\text{tot}}$ is constant, and thus, that the derivative $\dot{\mathbf{J}}_{\text{tot}}$ is equal to $\dot{\mathbf{J}}_{\text{cmg}}$, the equations for the translational and rotational dynamics of the system can be obtained by substituting the expressions for linear and angular momentum into Kirchhoff's (5) as follows:

$$\begin{aligned} (m\mathbf{I} + \mathbf{M}_A)\dot{u} &= -\omega \times \mathbf{P} + F_{\text{ext}} \\ (\mathbf{J}_{\text{tot}} + \mathbf{J}_A)\dot{\omega} &= -\dot{\mathbf{J}}_{\text{cmg}}\omega - \omega \times \mathbf{\Pi} - u \times \mathbf{P} - \tau_{\text{cmg}} + \tau_{\text{ext}} \end{aligned} \tag{8}$$

where no dynamic terms have been omitted. The first two terms on the right of (8) describe the coupled effects of CMG motion and the rotation of the body. The third term describes the coupled effects of the translational dynamics on body rotation. The fourth term, described by (4), accounts for the gimbal input and gyroscopic output torques of the CMG system. The spin axis dynamics of the CMGs have no contribution as the angular velocity of the flywheels is constant during operation. The final term accounts for any externally applied forces and moments, which for a body with zero righting moment is due to other actuators and viscous hydrodynamic interactions

$$\begin{aligned} F_{\text{ext}} &= F_u + F_{\text{drag}} \\ \tau_{\text{ext}} &= \tau_{\text{drag}}. \end{aligned}$$

It is reasonable to assume that for this application external actuators are arranged to have no resultant torque effect.

C. Viscosity

While the technology exists to analytically solve the Navier–Stokes equations and determine the exact effects of the hydrodynamic interactions, such calculations require sophisticated computational fluid dynamics (CFD) packages and powerful computers and even then can take several days to solve. Therefore, with current technology, these equations are not suitable for application onboard AUVs since they must determine the effects of drag in real time and so empirical models must be relied upon. While these models cannot predict with great accuracy all the interactions of an unsteady, 3-D flow regime over a self-propelled underwater body, they can capture the essential elements of flow and provide an effective tool to approximate the hydrodynamic forces that act on the body. The viscous drag can be expressed by the following standard empirical model:

$$F_{\text{drag}} = -\frac{1}{2}\rho A_i C_{Di} u|u|$$
$$\tau_{\text{drag}} = -\frac{1}{2}\rho \sum A_i C_{Di} r_i^3 \omega|\omega|$$

where ρ is the density of the surrounding fluid, A_i is the matrix of projected cross-sectional areas of the body, C_{Di} is the drag coefficient of the body, and r_i is the mean distance to the center of rotation. The drag coefficient of the robot can be calculated based on the various 3-D shapes that make up its hull [15].

D. Conversion to Inertial Frame

For unrestricted attitude control, the mathematical description of attitude must not possess any numerical singularities. Therefore, a four-parameter quaternion method based on Euler parameters is used to describe the orientation of the body in the inertial frame. The quaternion is defined as

$$\mathbf{q} = \begin{pmatrix} \xi_i \\ \xi_j \\ \xi_k \\ \eta \end{pmatrix} = \begin{pmatrix} \boldsymbol{\lambda} \sin\dfrac{\beta}{2} \\ \cos\dfrac{\beta}{2} \end{pmatrix}$$

where the angle $\boldsymbol{\beta}$ is the angle of simple rotation about the axis $\boldsymbol{\lambda} = [\lambda_i, \lambda_j, \lambda_k]^T$ that would bring the body frame back to the inertial frame. The derivative of the quaternion can be written as

$$\dot{\mathbf{q}} = Q(\mathbf{q})\omega \tag{9}$$

where the coordinate transformation matrix is

$$Q(\mathbf{q}) = \frac{1}{2}\begin{pmatrix} \eta & -\xi_k & \xi_j \\ \xi_k & \eta & -\xi_i \\ -\xi_j & \xi_i & \eta \\ -\xi_i & -\xi_j & -\xi_k \end{pmatrix}.$$

IV. Control Law

In an uncertain and constantly changing environment such as the ocean, it is important to ensure that unforeseen disturbances do not cause significant degradation in subsequent control performance. Lyapunov's direct method assesses stability by considering the time variation of a scalar energy-like function of the nonlinear system. If engineering insight and physical properties are exploited, a Lyapunov analysis can allow for elegant and powerful control solutions to even the most complex problems [16].

The role of the CMGs is analogous to a system of nonlinear springs and dampers that bring the body smoothly to its desired state. This analogy is formalized by defining the following Lyapunov function based on potential and kinetic energy-like terms with respect to the desired state, similar to that chosen by Oh [17] but extended to take into account the effects of added fluid inertia:

$$V(\mathbf{e}_q, \mathbf{e}_\omega) = \frac{1}{2}\mathbf{e}_q^T k_q \mathbf{e}_q + \frac{1}{2}\mathbf{e}_\omega^T(\mathbf{J}_{\text{tot}} + \mathbf{J}_A)\mathbf{e}_\omega \tag{10}$$

where $\mathbf{e}_q = \mathbf{q} - \mathbf{q}_d$ and $\mathbf{e}_\omega = \omega - \omega_d$ are the attitude and angular velocity errors with respect to the desired state. Since k_q is a diagonal matrix of positive gains and the inertia of the system is always positive and nonzero, the Lyapunov function is positive definite and the following conditions are satisfied:

$$V(\mathbf{e}_q, \mathbf{e}_\omega) > 0 \quad \text{for} \quad [\mathbf{e}_q, \mathbf{e}_\omega] \neq [0, 0]$$
$$V(\mathbf{e}_q, \mathbf{e}_\omega) \to \infty \quad \text{as} \quad |\mathbf{e}_q, \mathbf{e}_\omega| \to \infty.$$

The time derivative of the Lyapunov function can be obtained by differentiating (10) to give the following expression:

$$\dot{V}(\mathbf{e}_q, \mathbf{e}_\omega) = \mathbf{e}_q^T k_q \dot{\mathbf{e}}_q + \frac{1}{2}\mathbf{e}_\omega^T \dot{\mathbf{J}}_{\text{tot}} \mathbf{e}_\omega + \mathbf{e}_\omega^T \mathbf{J}_{\text{tot}} \dot{\mathbf{e}}_\omega.$$

Using the relationship in (9) to express $\dot{\mathbf{e}}_q$ and recalling that $\dot{\mathbf{J}}_{\text{tot}} = \dot{\mathbf{J}}_{\text{cmg}}$ gives

$$\dot{V}(\mathbf{e}_q, \mathbf{e}_\omega) = \mathbf{e}_q^T k_q Q(\mathbf{q})\mathbf{e}_\omega + \frac{1}{2}\mathbf{e}_\omega^T \dot{\mathbf{J}}_{\text{cmg}} \mathbf{e}_\omega + \mathbf{e}_\omega^T \mathbf{J}_{\text{tot}} \dot{\mathbf{e}}_\omega.$$

Since the product in the first term equates to a scalar value

$$\mathbf{e}_q^T k_q Q(\mathbf{q})\mathbf{e}_\omega = \left[\mathbf{e}_\omega^T Q^T(\mathbf{q}) k_q^T \mathbf{e}_q\right]^T = \left[\mathbf{e}_\omega^T Q^T(\mathbf{q}) k_q \mathbf{e}_q\right]$$

the derivative can be written in the following form:

$$\dot{V}(\mathbf{e}_q, \mathbf{e}_\omega) = \mathbf{e}_\omega^T \left[Q^T(\mathbf{q}) k_q \mathbf{e}_q + \frac{1}{2}\dot{\mathbf{J}}_{\text{cmg}} \mathbf{e}_\omega + (\mathbf{J}_{\text{tot}} + \mathbf{J}_A)\dot{\mathbf{e}}_\omega \right].$$

The Lyapunov derivative can only be guaranteed negative by choosing the relationship

$$k_\omega \mathbf{e}_\omega = -\left[Q^T(\mathbf{q}) k_q \mathbf{e}_q + \frac{1}{2}\dot{\mathbf{J}}_{\text{cmg}} \mathbf{e}_\omega + (\mathbf{J}_{\text{tot}} + \mathbf{J}_A)\dot{\mathbf{e}}_\omega \right] \tag{11}$$

where k_ω is a diagonal matrix of positive gains. Thus, the Lyapunov derivative becomes

$$\dot{V}(\mathbf{e}_q, \mathbf{e}_\omega) = -\mathbf{e}_\omega^T k_\omega \mathbf{e}_\omega \leq 0 \quad \text{for} \quad [\mathbf{e}_q, \mathbf{e}_\omega] \neq [0, 0]. \tag{12}$$

This describes the energy dissipated by the system. It can be seen that the system would be in equilibrium (i.e., $\dot{V} = 0$) anywhere along $\mathbf{e}_\omega = 0$ even if $\mathbf{e}_q \neq 0$, and thus, the Lyapunov derivative is only negative semidefinite. Although this ensures the stability of the system, further analysis is required to show that the system will also converge to the desired state.

In control systems where the Lyapunov derivative is only negative semidefinite, it is still possible to draw conclusions

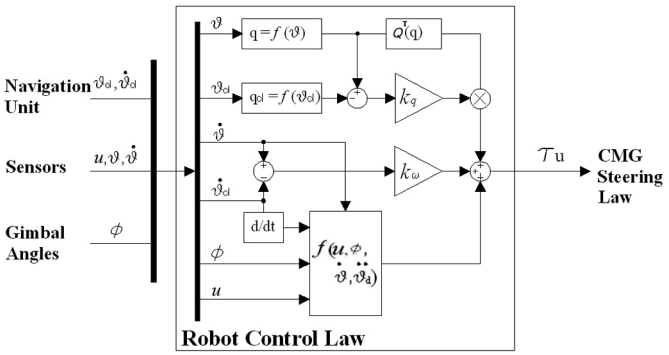

Fig. 4. Attitude control law for CMG-actuated underwater robots: The control law computes the torques required to achieve the desired robot state, taking into account the coupled dynamics of the CMG, body, and fluid system.

on asymptotic stability by applying the invariance principle of La Salle to formulate a control law that ensures the origin $[\mathbf{e}_\omega, \mathbf{e}_q] = [0,0]$ is the largest invariant set in $\dot{V}(\mathbf{x}) = 0$ [16]. Such a control law can be developed by first rearranging (11) to express the angular acceleration of the body in terms of the gains k_q and k_ω as follows:

$$(\mathbf{J}_{\rm tot} + \mathbf{J}_A)\dot{\omega} = -k_\omega \mathbf{e}_\omega - Q^T(\mathbf{q}) k_q \mathbf{e}_q + \frac{1}{2}\dot{\mathbf{J}}_{\rm cmg}(\omega_d - \omega) + (\mathbf{J}_{\rm tot} + \mathbf{J}_A)\dot{\omega}_d.$$

Substituting this expression into the equations for the rotational dynamics derived in (8) gives the condition

$$Q^T(\mathbf{q}) k_q \mathbf{e}_q + k_\omega \mathbf{e}_\omega - \frac{1}{2}\dot{\mathbf{J}}_{\rm cmg}(\omega + \omega_d) - (\mathbf{J}_{\rm tot} + \mathbf{J}_A)\dot{\omega}_d - \omega \times \mathbf{\Pi} - u \times \mathbf{P} - \tau_{\rm cmg} + \tau_{\rm drag} = 0.$$

Substituting in the expressions for $\tau_{\rm cmg}$ in (4) and $\dot{\mathbf{J}}_{\rm cmg}$ in (3) allows the equation to be expressed in the form

$$\mathbf{G}\ddot{\phi} - \mathbf{C}\dot{\phi} = \tau_u \tag{13}$$

where $\mathbf{C}$ fully describes the nonlinear first-order dynamics of a CMG cluster in a rigid body and $\mathbf{G}$ accounts for the inertia of the CMGs about the gimbal axes. Based on this expression, the control law is formulated as

$$\tau_u = Q^T(\mathbf{q}) k_q \mathbf{e}_q + [k_\omega \mathbf{e}_\omega - (\mathbf{J}_{\rm tot} + \mathbf{J}_A)\dot{\omega}_d - \omega \times \mathbf{\Pi} - u \times \mathbf{P} + \tau_{\rm drag}]. \tag{14}$$

This control law computes the torques required to achieve the desired robot state, where the sensitivity is tuned by the attitude and angular rate gains k_q and k_ω. The first term acts like a spring to bring the robot to the desired state and the remaining bracketed terms constitute a dissipative term to achieve smooth and continuous motion. This attitude control law is illustrated in Fig. 4. Letting $\tau_u = \tau_{\rm cmg}$ in the dynamic (8) gives the following condition:

$$(\mathbf{J}_{\rm tot} + \mathbf{J}_A)\dot{\mathbf{e}}_\omega + k_\omega \mathbf{e}_\omega + Q^T(\mathbf{q}) k_q \mathbf{e}_q + \left[\left(h_1 c_1^T + c_1 h_1^T\right)\omega \ldots \left(h_N c_N^T + c_N h_N^T\right)\omega\right](\mathbf{J}_c - \mathbf{J}_h)\dot{\tilde{\phi}} = 0.$$

This indicates that, for the system to remain in stable equilibrium where $\mathbf{e}_\omega \equiv \dot{\mathbf{e}}_\omega \equiv 0$, it is possible to guarantee $\mathbf{e}_q \equiv 0$ by ensuring that $\dot{\tilde{\phi}} = 0$; i.e., the CMGs do not produce any torque. This is in fact a trivial condition since any actuating effect at this point would drive the system away from its desired state. This is satisfied by the candidate control law since when the system is in equilibrium at the origin $[\mathbf{e}_q, \mathbf{e}_\omega] = [0,0]$ the torque computed by the control law is zero and so the gimbals are stationary; i.e., $\dot{\tilde{\phi}} = 0$. The analysis shows that the control law (14) ensures $\dot{V} \equiv 0$ only at the equilibrium point $\mathbf{e}_\omega \equiv \mathbf{e}_q \equiv 0$ since $[\mathbf{e}_q, 0]$ is the set of all points where $\dot{V}(\mathbf{x}) = 0$ and $[0,0]$ is the largest invariant set in $[\mathbf{e}_q, 0]$. Thus, the system satisfies the conditions of La Salle's invariance principle and guarantees the global asymptotic stability of the system to the desired state. In contrast to all previous CMG applications, the control law developed in this research takes into account the effects of translation and the hydrodynamic interactions of the body as well as the coupled dynamics of the CMG and body system.

V. Singularities and Null Motion

A. Singularity Problem

The singularity problem for single gimbal systems was first identified by the National Aeronautics and Space Administration (NASA) in 1972 [18]. A singularity occurs when all the momentum vectors of the CMG system become coplanar. The system becomes unable to generate torque about the parallel axis and this can result in a momentary loss of control authority. These singularities must be avoided to achieve smooth and continuous attitude control. The most basic CMG steering law makes the reasonable assumption that the stored momentum is large; i.e., $\mathbf{C} \gg \mathbf{G}$. Thus, the second-order term in (13) becomes negligible and a particular solution for the desired torque can be computed by taking the pseudoinverse of the $[N \times 3]$ Jacobian $\mathbf{C}$

$$\dot{\tilde{\phi}}_\tau = -\mathbf{C}^T(\mathbf{C}\mathbf{C}^T)^{-1}\boldsymbol{\tau}_u. \tag{15}$$

However, the pseudoinverse produces a minimum norm vector, implying that, once in its vicinity, a CMG unit will oscillate at an unreasonably high gimbal rate about the norm and become stuck in this direction. Although this has little effect on the torque generated, this behavior encourages the formation of coplanar singular orientations.

B. Redundancy and Null Motion

The solution to the singularity problem lies in the system's null motion. Margulies [19] was the first to identify null motion and the possibility of singularity avoidance in redundant systems. Systems with more CMG units than controlled degrees of freedom have a dimensional redundancy that allows for motion of the gimbals by which all the momentum vectors exactly cancel and so no resultant torque is produced. This null motion can be used to avoid singular orientations to some extent. Whether complete singularity avoidance is possible depends on the degree of redundancy and how it is used. The linear combination of the inverse steering solution and null motion forms the general relationship that describes all possible CMG motions to exactly achieve a specific command torque

$$\dot{\tilde{\phi}}_d = \dot{\tilde{\phi}}_\tau + k_{\rm null}\dot{\tilde{\phi}}_Z.$$

This forms the basis of all singularity avoidance steering laws. However, difficulties arise from attempting to manipulate a

cluster of single degree-of-freedom actuators to control motion about multiple axes. This limits the dimensions of null motion, which for three-axis control has an order of $N-3$. Tokar [20] proved that only a system with six or more CMG units has enough redundancy to solve the singularity problem. This led to the construction of a six-unit system for the Russian space station MIR [14]. However, increased redundancy comes at the cost of the size and complexity of the system and it is not practical for underwater applications where strict dimensional, mass, and computational restrictions apply. Conversely, a system of three units has no redundancy and so its singular orientations cannot be avoided. Therefore, a method to guarantee singularity avoidance in a system of minimal redundancy, specifically the CMG pyramid, is sought.

VI. Geometric Analysis of Singularities

A. Singular Surfaces

After the initial work of Margulies [19] and Tokar [20], geometric studies by Kurokawa [21] and Paradiso [22] have formed a deeper understanding of the singularity problem and provided a useful tool for the analysis of potential solutions. At a singularity, the transverse matrix $\bar{c}$ is not of full rank and it becomes possible to define the normal unit vector

$$\mathbf{u} = c_i \times c_j, \qquad \text{where} \quad i \neq j.$$

The singular angular momentum vectors can be expressed in terms of $\mathbf{u}$ as follows [21]:

$$\bar{h}_S = \sum_{i=1}^{N} \epsilon_i \frac{(g_i \times \mathbf{u}) \times g_i}{|g_i \times \mathbf{u}|}. \tag{16}$$

This equation represents a mapping from the singular orientations to the smooth and continuous surface of singular momentum vectors S_ϵ where

$$S_\epsilon = \{\bar{h}_S : \forall\, c_{Si}\mathbf{u} = 0, \ \text{where} \ i = 1, 2, \ldots, N\}.$$

The singular surface can be classified into regions by the sign variable ϵ_i that represents the relative orientation of each unit. If the direction of the units and the singular direction vector are reversed, i.e., $\epsilon \rightarrow -\epsilon$ and $\mathbf{u} \rightarrow -\mathbf{u}$, the angular momentum $\bar{h}_S$ remains the same, and thus, the surface regions S_ϵ and $S_{-\epsilon}$ are identical. Therefore, there are a total of $2N-1$ different singular regions. However, not all singularities can be avoided through null motion alone and so the implications for CMG steering can only be understood by distinguishing singularities that are as follows:

- escapable through null motion;
- inescapable through null motion.

Although escapable singularities can be avoided without any undesired torque effects, inescapable singularities cannot be physically avoided without generating an error in torque [20]. These can be classified using the geometric escapability condition formulated by Kurokawa [21] that discriminates between different types of singularities based on the differential geometry of null motion.

B. Differential Geometry and Escapability

The effects of infinitesimal changes in gimbal angle on the singular angular momentum vector can be determined by taking a second-order Taylor series expansion near the singular orientation $\bar{\phi}_S$

$$\bar{h}(\bar{\phi}_S + d\bar{\phi}) = \bar{h}(\bar{\phi}_S) + \sum_{i=1}^{N} \frac{\partial \bar{h}}{\partial \phi_i} d\phi_i + \frac{1}{2} \sum_{i=1}^{N} \sum_{j=1}^{N} \frac{\partial^2 \bar{h}}{\partial \phi_i \partial \phi_j} d\phi_i d\phi_j$$

where terms of third-order and greater have been omitted. The change in angular momentum can be obtained

$$\begin{aligned} \Delta\bar{h} &= \bar{h}(\bar{\phi}_S + d\bar{\phi}) - \bar{h}(\bar{\phi}_S) \\ &= \sum_{i=1}^{N} \frac{\partial \bar{h}}{\partial \phi_i} d\phi_i + \frac{1}{2} \sum_{i=1}^{N} \sum_{j=1}^{N} \frac{\partial^2 \bar{h}}{\partial \phi_i \partial \phi_j} d\phi_i d\phi_j. \end{aligned}$$

The first partial derivative is c_i by definition (1). At a singularity, the following conditions are also satisfied

$$\begin{aligned} \frac{\partial^2 \bar{h}}{\partial \phi_i \partial \phi_j} &= -h_i, \qquad \text{if} \quad i = j \\ \frac{\partial^2 \bar{h}}{\partial \phi_i \partial \phi_j} &= 0, \qquad \text{if} \quad i \neq j. \end{aligned}$$

The change in angular momentum can be expressed as

$$\Delta\bar{h} = \sum_{i=1}^{N} c_i d\phi_i - \frac{1}{2} \sum_{i=1}^{N} h_i (d\phi_i)^2$$

where by definition the first-order term is orthogonal to $\mathbf{u}$. Postmultiplying by $\mathbf{u}$ and expressing the variable in the orthogonal components of its null and singular tangent subspaces gives

$$\Delta\bar{h}\mathbf{u} = -\frac{1}{2} d\bar{\phi}_S^T P^{-1} d\bar{\phi}_S - \frac{1}{2} d\bar{\phi}_Z^T P^{-1} d\bar{\phi}_Z$$

where $P = 1/(\mathbf{u} \cdot \bar{h})$. The two components of the quadratic are orthogonal and so can be treated independently

$$\begin{aligned} Q_S &= -\frac{1}{2} d\bar{\phi}_S^T P^{-1} d\bar{\phi}_S \\ Q_Z &= -\frac{1}{2} d\bar{\phi}_Z^T P^{-1} d\bar{\phi}_Z \end{aligned} \tag{17}$$

where Q_S expresses the curvature of the singular surface and Q_Z represents the shape of null motion that steers the gimbals away from singular orientations. The signature of Q_Z defines the escapability of the singularity. Since P^{-1} cannot be zero, all the singular points are either of the following:

- escapable—if Q_Z is indefinite;
- inescapable—if Q_Z is definite.

If Q_Z is indefinite, null motion is open ended, existing on both sides of the singularity as well as on the singularity itself. This means that the singularity is escapable through null motion alone and the gimbals can be steered away from it without generating any undesired torque effects. If in contrast Q_Z is definite, null motion is closed, existing only on one side of the singularity. Furthermore, the system's null motion collapses into the singular point with no null motion at the singularity

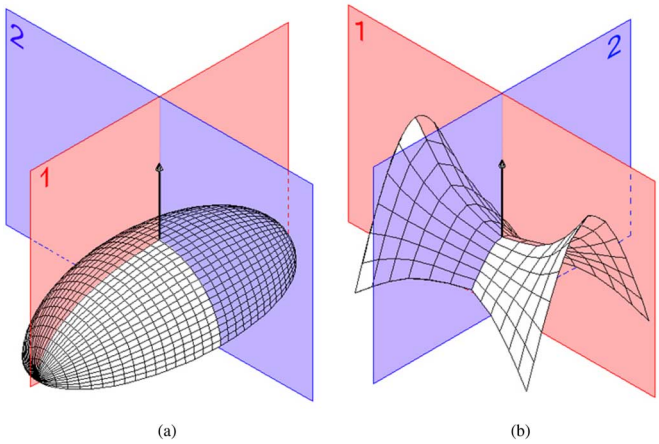

Fig. 5. (a) Elliptic and (b) hyperbolic null motion: The curvature of null motion about a singularity is either elliptic or hyperbolic. This can be determined by comparing the maximum and minimum principal curvatures shown in planes 1 and 2, respectively, where the convention has been adopted that inward curvature is positive.

itself. Therefore, once near this kind of inescapable singularity, it cannot be crossed or avoided without generating undesired torque effects.

The signature of Q_Z can be determined through the sign of its Gaussian curvature K, which indicates the shape of null motion about the singular point. This can be obtained from the maximal and minimal extremes of curvatures $[\kappa_1, \kappa_2]$, or principal curvatures of null motion, as visualized in Fig. 5. The Gaussian curvature can be calculated by taking the product of the principal curvatures

$$K = \kappa_1 \kappa_2.$$

If K is positive, the principal curvatures have the same sign and so the shape of null motion must be elliptic [Fig. 5(a)], terminating at the singular point. This form of null motion indicates that the signature of Q_Z is definite. If K is negative, the principal curvatures have different signs and so the shape of null motion must be hyperbolic [Fig. 5(b)], bifurcating at the singular point. This form of null motion indicates that the signature of Q_Z is indefinite.

The null element $d\bar{\phi}_Z$ of the tangent subspace is derived using the vectors of the singular system c_{S1}, c_{S2}, c_{Si}, and $\mathbf{u}$ using the following general expression for four arbitrary vectors in 3-D space

$$\begin{aligned} &c_{S1}[\,c_{S2} \quad c_{Si} \quad \mathbf{u}\,] - c_{S2}[\,c_{Si} \quad \mathbf{u} \quad c_{S1}\,] \\ &\quad + c_{Si}[\,\mathbf{u} \quad c_{S1} \quad c_{S2}\,] - \mathbf{u}[\,c_{S1} \quad c_{S2} \quad c_{Si}\,] \\ &\quad = 0, \qquad \text{where} \quad i = 3, \ldots, N. \end{aligned}$$

Since the singular torque vectors c_{S1}, c_{S2}, and c_{Si} lie on the same plane, the final term becomes zero. The triple scalar products can be rearranged to give

$$\begin{aligned} c_{S1}[\,c_{S2} \quad c_{Si} \quad \mathbf{u}\,] + c_{S2}[\,c_{Si} \quad c_{S1} \quad \mathbf{u}\,] \\ + c_{Si}[\,c_{S1} \quad c_{S2} \quad \mathbf{u}\,] = 0. \end{aligned}$$

Defining $n_{i,j} = [\,c_{Si} \quad c_{Sj} \quad \mathbf{u}\,]$ gives the condition

$$n_{2,i} c_{S1} + n_{i,1} c_{S2} + n_{1,2} c_{Si} = 0.$$

This forms a candidate for the basis of the null subspace. This has an order of $N-2$, where the null element can be expressed in terms of the candidate basis as follows:

$$d\bar{\phi}_Z = z_1 e_{Z1} + z_2 e_{Z2} + \cdots + z_{(N-2)} e_{ZN-2} = E_Z \bar{z}$$

where $\bar{z}$ is a $[(N-2) \times 1]$ vector and E_Z is the $[N \times (N-2)]$ null subspace matrix

$$E_Z = \begin{bmatrix} n_{2,3} & n_{3,1} & n_{1,2} & 0 & \ldots & 0 \\ n_{2,4} & n_{4,1} & 0 & n_{1,2} & \ldots & 0 \\ \vdots & \vdots & \vdots & \vdots & \ddots & \vdots \\ n_{2,(N-2)} & n_{(N-2),1} & 0 & 0 & \ldots & n_{1,2} \end{bmatrix}.$$

Substituting the basis into the expression for Q_Z in (17) gives

$$Q_Z = -\frac{1}{2} \bar{z}^T E_Z^T P^{-1} E_Z \bar{z}.$$

The signature of Q_Z is independent of the variable $\bar{z}$ and so is defined by the matrix

$$A_Z = E_Z^T P^{-1} E_Z$$

where A_Z is an $[N \times N]$ matrix with maximum and minimum eigenvalues that represent the principal curvatures $[\kappa_1, \kappa_2]$. Thus, the Gaussian curvature of null motion can be determined for all singular orientations as follows:

$$K = \kappa_1 \kappa_2 = \max[\text{eig}(A_Z)] \min[\text{eig}(A_Z)]. \tag{18}$$

This term does not vanish as P^{-1} cannot be zero. Therefore, every singular orientation can be classified based on the following condition:

- if $K < 0$, the singularity is escapable, else
- if $K > 0$, the singularity is inescapable.

C. Singularities of a CMG Pyramid

The mathematical tools developed are used to perform a comprehensive geometric study of the singularities of a four-unit CMG pyramid (Fig. 6). The null motion of this minimally redundant system can be computed for each unit by taking the scalar triple product of the remaining torque vectors [19]

$$\begin{aligned} \dot{\bar{\phi}}_Z = [[\,c_2 \quad c_3 \quad c_4\,], -[\,c_3 \quad c_4 \quad c_1\,], \\ [\,c_4 \quad c_1 \quad c_2\,], -[\,c_1 \quad c_2 \quad c_3\,]]^T. \end{aligned}$$

The null motion $\dot{\bar{\phi}}_Z$ is orthogonal to the torque matrix $\bar{c}$. Since the nonsingular columns of $\bar{c}$ span 3-D space, the null motion of the four-unit system is 1-D.

The system has eight singular regions that are classified according to the number of reversed units whose momentum vectors face the negative direction [22]. Figs. 7–11 show the singular surface for a skew angle of $\beta = \cos^{-1}(1/\sqrt{3})$, which has a near-spherical momentum envelope and so equal control authority about all three rotational degrees. The figures are generated by mapping a polar lattice of singular orientations to their corresponding angular momentum vectors using (16). Escapable and inescapable areas are distinguished using (18). For clarity of presentation, inescapable areas are plotted alongside the complete singular surface regions where appropriate.

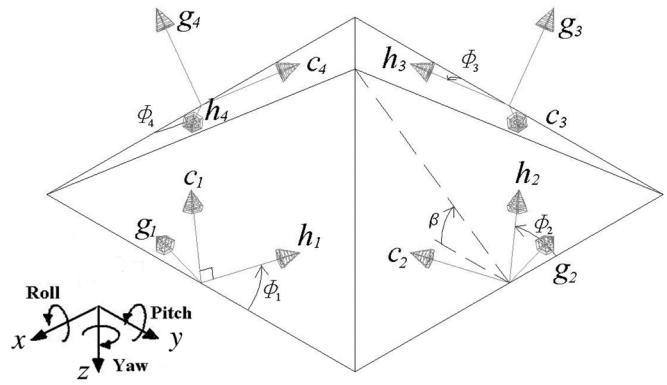

Fig. 6. CMG pyramid: The pyramid configuration is a nonparallel-type CMG system that consists of four units arranged symmetrically about its center. The gimbal axis of each unit lies normal to the surface of a pyramid with a skew angle of β. The symmetrical nature is convenient for attitude control as it allows independent actuation about all three rotational axes. However, with only four units, the system is minimally redundant and this poses significant challenges for singularity avoidance.

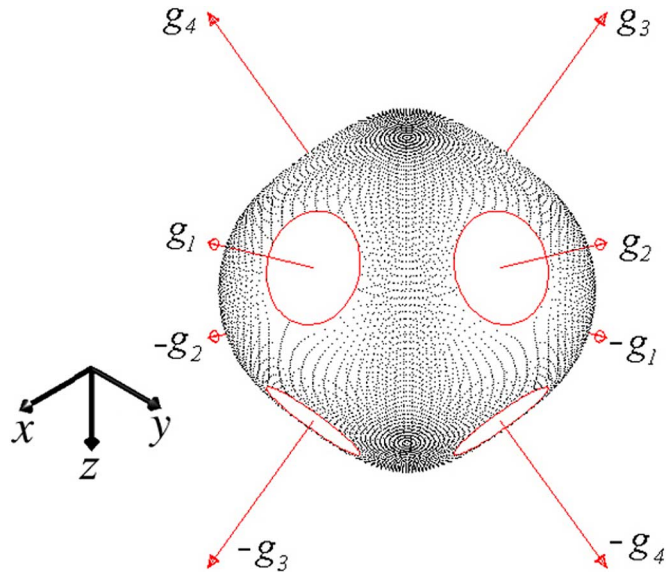

Fig. 7. Isometric view of S_{++++}: This external singular region represents the maximum amplitude of the momentum stored in the system.

1) Envelope: The surface region S_{++++}, shown in Fig. 7, forms a spherical envelope that represents the boundary of the momentum workspace. This region represents the maximum amplitude of the momentum stored in the system and so the entire surface region is trivially inescapable. As the momentum vectors rotate about the gimbal axes where $\mathbf{u} = \pm g_i$, eight-unit circles are formed that appear as holes in the surface.

2) Outer Zone: The outer singular zone is composed of the four regions S_{-+++}, S_{+-++}, S_{++-+}, and S_{+++-} that can be mapped onto each other by a series of 90° rotations about the z-axis. Fig. 8 shows the regions S_{-+++} and S_{++-+}. The petal shapes fill the holes in Fig. 7 and form part of the external envelope. The inescapable areas penetrate some way into the momentum workspace.

3) Inner Zone: Regions with two negative ϵ_i form the inner singular zone. These regions form the smallest part of the singular surface that fits within the outer singular zone and has no part in contact with the external envelope. Fig. 9 shows the regions S_{--++} and S_{+--+} that are formed when adjacent units are reversed. The region formed by reversing opposite units is shown in Fig. 10. These regions form complex ridged shapes that join the strips of the outer singular zone (Fig. 8).

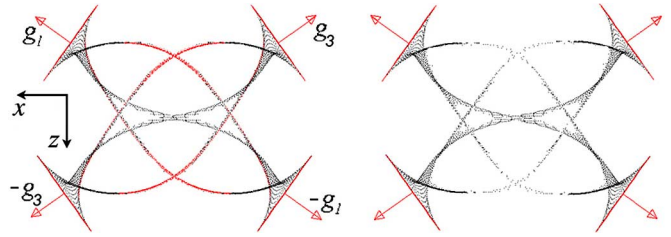

Fig. 8. The xz-plane view of S_{-+++} and S_{++-+}: Each region forms a petal aligned with the reversed gimbal axis. These develop three thin strips that twist along the gimbal axis, intersecting at six regularly spaced nodes about the momentum origin, to form another symmetrical petal.

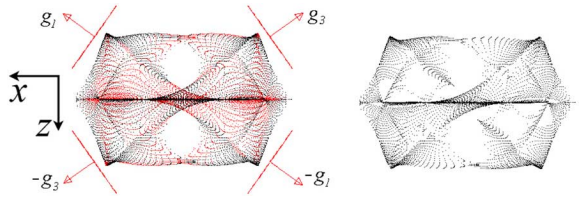

Fig. 9. The xz-plane view of S_{--++} and S_{+--+}: The inescapable areas of these regions are heavily concentrated along the xy-plane.

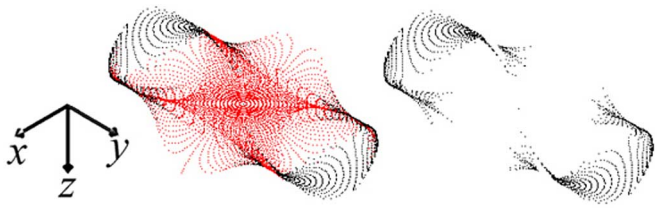

Fig. 10. Isometric view of S_{-+-+}: This region is mostly escapable, only becoming inescapable towards its extremities.

4) Complete Surface: The singular regions of a minimally redundant CMG pyramid join to form a smooth and continuous surface of singular momentum vectors of closed form, as shown in Fig. 11. Although there exist large volumes with no singularities, inescapable areas penetrate deeply into the momentum space in a complex manner, enclosing the origin with a significant concentration on the xy-plane. This has serious implications for attitude control, in particular, degrading control about the roll and pitch axes. The analysis shows that the minimally redundant system contains inescapable singularities through which no steering law can remain exact.

VII. Singularity Avoidance Steering Law

A. Singularity Avoidance

The singularity problem applies to any system with limited redundancy that aims to perform exact and real-time steering. Furthermore, the likelihood of encountering singularities is increased as sustained torques are required to overcome the viscous resistance of the fluid. Although singularity avoidance can be achieved by relaxing the exactness and real-time constraints [22]–[24], the behavior of an AUV cannot be foreseen since they

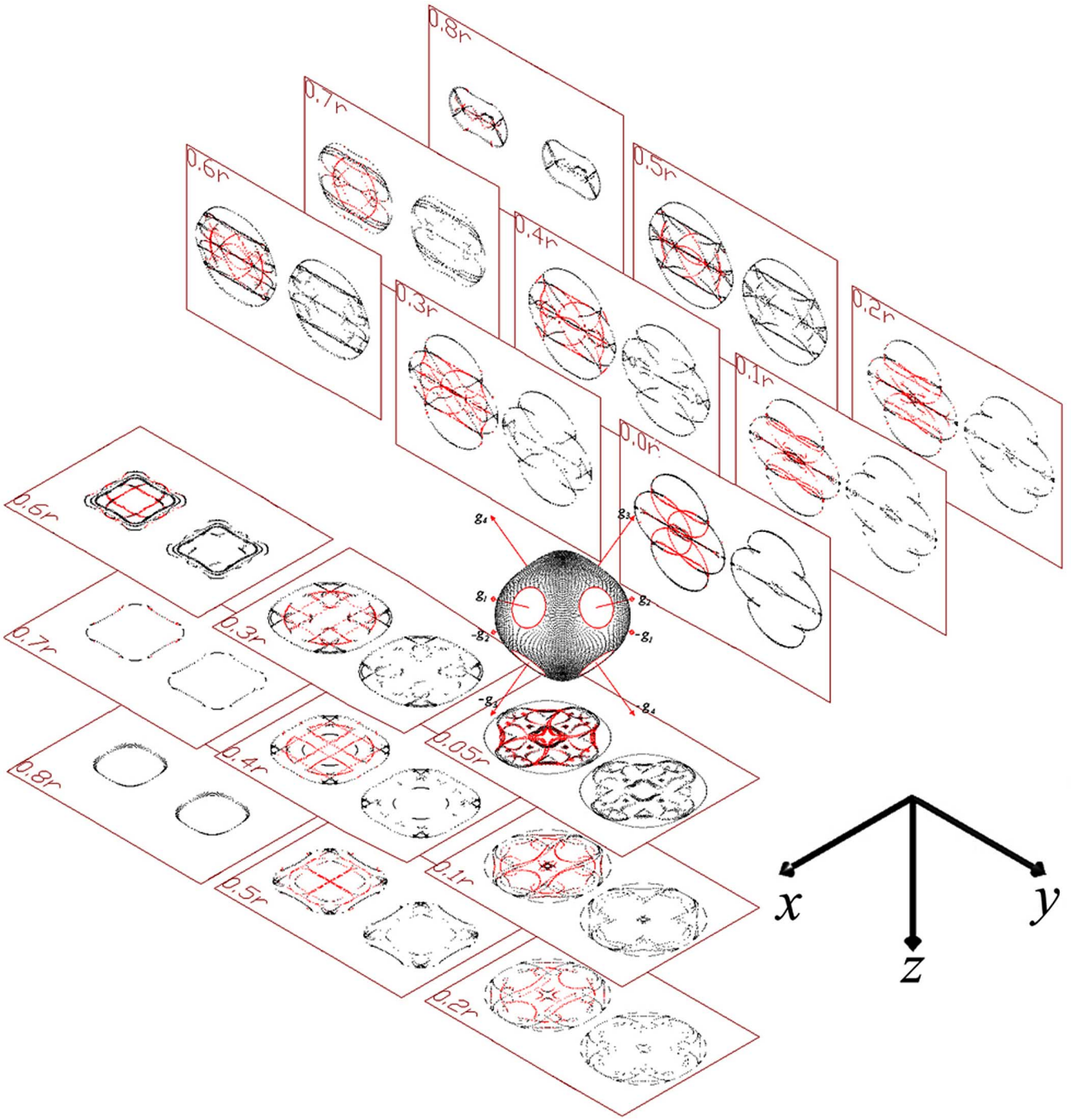

Fig. 11. Exploded view of the complete singular surface of a CMG pyramid: The different regions join to form a smooth and continuous closed surface of singular momentum vectors. Various cross sections of this surface are projected in the x- and z-directions. The complex distribution of inescapable singularities cannot be easily overcome by real-time steering and momentum management algorithms.

operate in an unknown environment using sensors to react to their surroundings where any error in actuation may endanger the safety of the robot. Therefore, a steering law for application to AUVs must be strictly real time and remain exact to the command. This can only be achieved by excluding all inescapable singularities from the workspace.

B. Inverse Kinematics and Workspace Restriction

Restriction of the momentum workspace reduces the torque available for control and so it is necessary to determine the largest continuous workspace that contains no inescapable singularities. Simply excluding all inescapable singularities from the workspace in Fig. 11 leaves only a small fraction of the momentum available for use and is too severe a restriction, resulting in an unacceptably inefficient use of the system. Therefore, instead of allowing the CMGs to steer freely, some rules of steering must be formulated to eliminate as many inescapable singularities as possible while keeping intact the largest viable volume of the workspace [21]. This is achieved by considering the inverse kinematics of attitude control with respect to the findings of the geometric analysis.

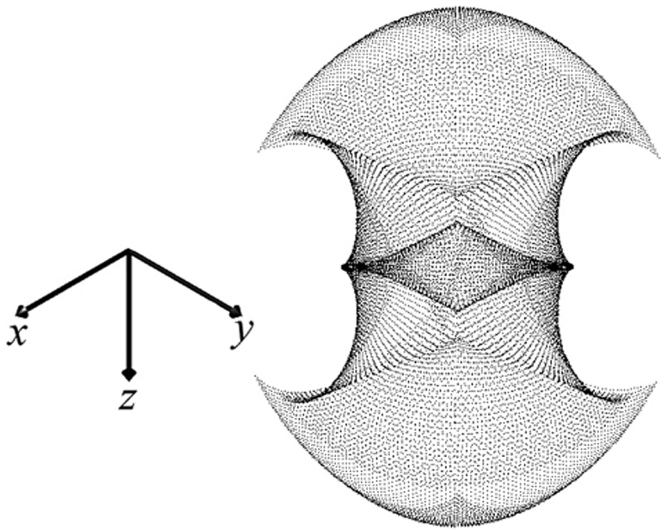

Fig. 12. Isometric view of the constrained workspace: The momentum envelope maintains its original dimension in the z-direction and maintains more than a third of its dimensions in the x- and y-directions.

The gyroscopic torque of the CMGs corresponds to the velocity of the angular momentum vector in 3-D momentum space and is generated about the path taken. If the nominal state is defined at the momentum origin, where all gimbal angles are zero, attitude control can be achieved by moving the momentum vector along a path parallel to its principal axes using the following steering commands:

$$\boldsymbol{\sigma} = \begin{bmatrix} \sigma \\ 0 \\ -\sigma \\ 0 \end{bmatrix}, \quad \boldsymbol{\gamma} = \begin{bmatrix} 0 \\ \gamma \\ 0 \\ -\gamma \end{bmatrix}, \quad \boldsymbol{\alpha} = \begin{bmatrix} \alpha \\ \alpha \\ \alpha \\ \alpha \end{bmatrix}$$

where the steering parameters σ, γ, and α independently govern roll, pitch, and yaw. These three steering parameters can be used to couple the motion of the four independent CMG units

$$\bar{\phi} = [\alpha + \sigma, \alpha + \gamma, \alpha - \sigma, \alpha - \gamma]^T. \tag{19}$$

This algebraically constrains gimbal motion by one degree of freedom and imposes the following restraining condition:

$$\phi_1 - \phi_2 + \phi_3 - \phi_4 = 0. \tag{20}$$

This eliminates many of the singular regions, simplifying the system's kinematics and globally restricting the workspace in a manner that is suitable for attitude control. The resulting constrained workspace is illustrated in Fig. 12 where some thin regions have been trimmed to allow for easier visualization.

The most important feature of this workspace is that the only inescapable singularities are those that form the boundary of the momentum envelope. This is a simple solution to the complex problem of singularity avoidance that guarantees exact and real-time steering by eliminating all internal singularities within a constrained workspace.

C. Global Steering Law

A global steering solution for exact and real-time singularity avoidance can be achieved by constraining the system to operate within the restricted workspace of Fig. 12. This can be implemented by formulating a steering law based on the parameters σ, γ, and α by applying relationship (19), which imposes the restraining condition (20). The solution for the desired torque in (15) becomes

$$\dot{\phi}^* = -(\mathbf{C}^*)^{-1}\boldsymbol{\tau}_u \tag{21}$$

where $\phi^* = [\sigma \quad \gamma \quad \alpha]^T$ and

$$\mathbf{C}^* = -2\mathbf{J}_h\dot{\bar{\psi}}\begin{bmatrix} \mathbf{c}\beta\mathbf{c}\alpha\mathbf{c}\sigma & -\mathbf{s}\alpha\mathbf{c}\gamma & -(\mathbf{c}\beta\mathbf{s}\alpha\mathbf{s}\sigma + \mathbf{c}\alpha\mathbf{s}\gamma) \\ \mathbf{s}\alpha\mathbf{c}\sigma & \mathbf{c}\beta\mathbf{c}\alpha\mathbf{c}\gamma & (\mathbf{c}\alpha\mathbf{s}\sigma - \mathbf{c}\beta\mathbf{s}\alpha\mathbf{s}\gamma) \\ -\mathbf{s}\beta\mathbf{s}\alpha\mathbf{s}\sigma & -\mathbf{s}\beta\mathbf{s}\alpha\mathbf{s}\gamma & (\mathbf{s}\beta\mathbf{c}\alpha\mathbf{c}\sigma + \mathbf{s}\beta\mathbf{c}\alpha\mathbf{c}\gamma) \end{bmatrix}$$

where $\mathbf{s}$ and $\mathbf{c}$ are abbreviations for $\sin$ and $\cos$. The Jacobian $\mathbf{C}^*$ is reduced to a $[3 \times 3]$ square matrix whose inverse can be calculated directly. For generalization, null motion can be superimposed through the null gain

$$k_{\text{null}} = -\kappa(\phi_1 - \phi_2 + \phi_3 - \phi_4)$$

where the sensitivity is tuned by adjusting κ. A schematic of the steering law is illustrated in Fig. 13.

VIII. Development of a Zero-G Underwater Robot

A. IKURA

IKURA, shown in Fig. 14, was constructed in June 2005 and is the first Zero-G class underwater robot. This is also, to the knowledge of the authors, the first application of CMGs to underwater robots. It should be noted that IKURA is a prototype, designed to provide an experimental platform to verify the theoretical developments presented and demonstrate the unique freedom in attitude control offered by CMGs, and thus, its specification primarily relates to control about the rotational axes. The CMGs must provide sufficient control authority from the nominal state so that the robot can do the following:

- rotate $\pm 180°$ in yaw, starting and finishing at rest in 6 s;
- rotate $\pm 90°$ in pitch, starting and finishing at rest in 3 s;
- stabilize any roll angle.

IKURA is made up of a cylindrical body with hemispherical ends. Its hull is small with a length of 0.5 m and a total mass of 17.0 kg. Since the CMGs are completely contained within the hull, they preserve its hydrodynamic integrity and maintain symmetry about its major axes, so that motion is essentially uncoupled between different degrees. Furthermore, the CMGs have no fluid interactions of their own, which greatly simplifies the hydrodynamic behavior of the robot. Details of the design are provided in Table I.

B. CMG System Design

IKURA contains a cluster of four CMG units that are arranged in a pyramid configuration, as shown in Fig. 15. A skew angle of $\beta = \cos^{-1}\sqrt{1/3}$ was chosen to provide greater control authority in yaw than in pitch when using the proposed steering law. The CMGs are sized based on the predictions of numerical simulations that used an optimized bang–bang control law. The minimum angular momentum required to meet the specification within the constrained workspace was computed to be 3.8 N·m·s with a maximum required torque of 0.47 N·m. Although it is desirable to have the flywheel rates as fast as possible, high speeds introduce practical problems such as vibration and wear in the bearings. Since the physical dimensions of the CMG system are

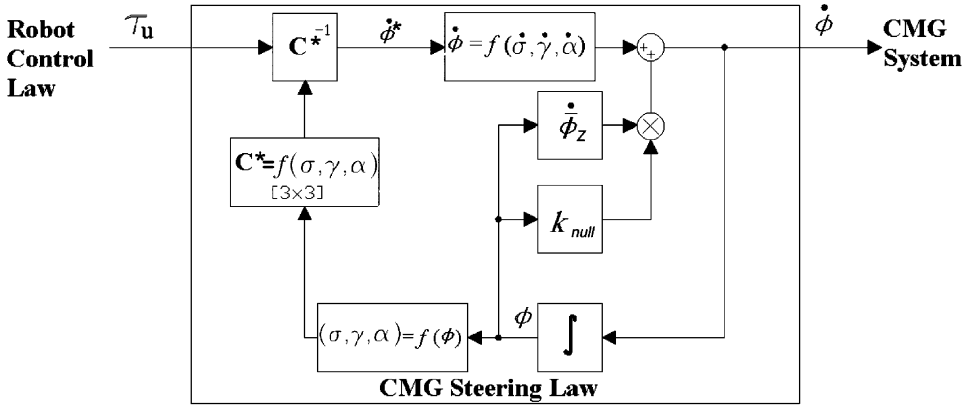

Fig. 13. Global steering law: This steering law operates within the constrained workspace of Fig. 12 and can be implemented in real-time applications while remaining exact to the control command.

Fig. 14. Zero-G class underwater robot IKURA: IKURA has coincident centers of gravity and buoyancy and is equipped with a CMG pyramid within its hull to provide unrestricted attitude control. A single thruster actuates surge so the robot can approach its missions in a truly 3-D manner.

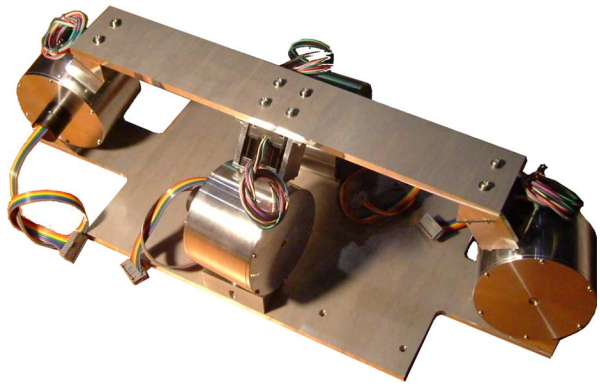

Fig. 15. CMG pyramid: The pyramid configuration provides independent roll, pitch, and yaw actuation. The shape of the pyramid is stretched to fit the pressure hull. However, angular symmetry is maintained about its center and so there are no detrimental effects on its performance as an actuator.

TABLE I
SPECIFICATION OF IKURA

IKURA parameter	Specification
Classification	Zero-G
Capabilities	Unrestricted attitude control and 3D missions
Objective	Investigate CMG and Zero-G applications
Hull [length, diameter]	[500, 220] mm
Mass	17.0 kg
Sensor	Attitude Heading Reference System (AHRS)
CPU	H8/3067 micro-controller
Translation	1× thruster (surge)
Rotation	CMG pyramid (roll, pitch, yaw)
Power consumption	20 W (∼ 100 W for acceleration)

limited by the space restrictions of the pressure hull, it is desirable for the flywheels to be made out of as dense a material as possible. However, the material must also be nonmagnetic and strong enough to withstand the large gyroscopic torques generated. A phosphorous-deoxidized copper alloy, with a density of 8900 kg·m^{-3}, was chosen as a suitable material. To ensure reliability, the system is designed to meet its specification at under 30% of its maximum rotational speed. A fast mechanical response and high resolution of control are achieved by using high torque servos to steer the gimbals. Keeping the steering law parameters in (19) within the range $\pm\pi/2$ limits the gimbal angles to $\pm 90°$. This is of significant practical importance as it guarantees the uniqueness of response and prevents multiple rotations of the gimbals. The latter point is often overlooked in simulations but would require complicated mechanisms for the actuation of the flywheels and serve no useful purpose. The parameters of the CMG system are specified in Table II.

IX. EXPERIMENTAL VERIFICATION

This section verifies the theoretical developments of this research and demonstrates the practical application of CMGs to Zero-G class underwater robots. A series of experiments is performed to assess the following:

- actuation capabilities of the CMG system;
- control and stabilization of the CMG, body, and fluid system.

To elucidate the first point, the torque generated by the CMG system was measured using an array of cantilevered strain gauges. For convenience of instrumentation, both experiments were performed on land. This does not make the results of the experiments any less valid since the torque generated by the CMG system is independent of its environment and is applied directly to the body of the robot. However, the robot's dynamic response is dependent on the environment and so

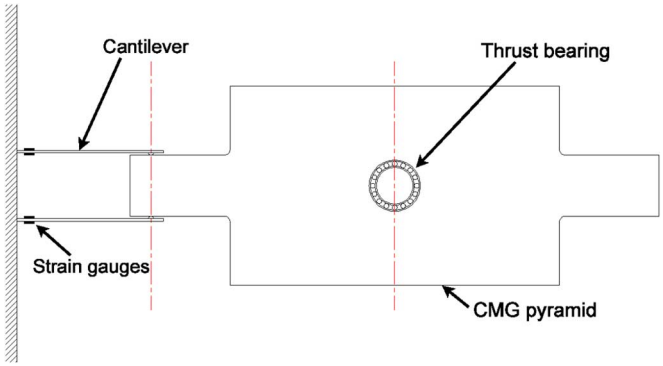

Fig. 16. Plan view of the CMG torque measurement setup: The torque generated is measured using an array of cantilevered strain gauges that were calibrated before each experiment. The CMG pyramid is mounted on a bearing so that it is free to rotate in yaw.

TABLE II
PHYSICAL PARAMETERS OF THE CMG PYRAMID

CMG parameter	Specification
Skew angle	54.7°
Gimbal torque	0.58 N·m (Futaba S9550)
Flywheel diameter	68 mm
Flywheel mass	825 g
Flywheel inertia	6.38×10^{-4} kg·m^2
Flywheel maximum rate	50 000 r/min (Maxon EC22-169007)
Output torque [roll, pitch, yaw]	$\sim [1, 1, 3]$ N·m
Maximum momentum stored	13.4 N·m·s
Maximum energy stored	35 kJ

the assessment of the control law was performed using the Zero-G prototype IKURA in the experimental pool facilities of the Underwater Robotics and Application (URA) laboratory, University of Tokyo, Tokyo, Japan.

A. CMG Actuation

The performance of CMGs as an actuator is assessed by measuring the torque generated by the CMG system and investigating the exactness and real-time applicability of the steering law. The experimental setup is illustrated in Fig. 16.

1) Gyroscopic Torque Output: The torque generated by the CMG system is measured and compared to that calculated online using (4). Fig. 17 shows the response of the system to a gimbal rate command of $\pm 8°$/s that covers the entire range of gimbal excursion angles. The flywheel rate $\dot{\psi}$ was set to 5000 r/min. The torque generated has a cosinusoidal relationship with the gimbal excursion angles and shows a good agreement to that computed online by the microcontroller. The 6.0% loss in magnitude is of an acceptable order considering mechanical disturbances such as friction, vibrations, and flywheel imbalance. The results confirm the dynamic equations derived for the CMG system.

2) Steering Law Exactness: The exactness and real-time applicability of the steering law in (21) is assessed by measuring the step response of the system to an open-loop torque command. Fig. 18 shows the response of the system to a command torque of 0.07 N·m for a flywheel rate of 5000 r/min. The steering law responds immediately to generate the command torque. The measured torque is maintained within 6.0% of that commanded until the system reaches the workspace envelope

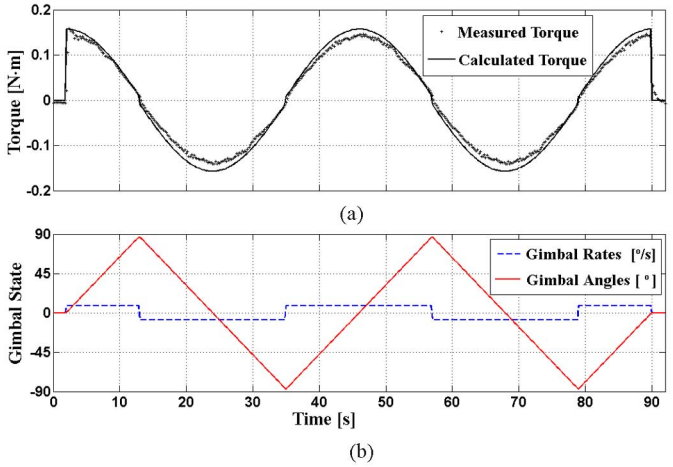

Fig. 17. Torque generated by the CMG system: (a) Comparison of the torque measured to that calculated online using (4). (b) Gimbal rates and gimbal excursion angles.

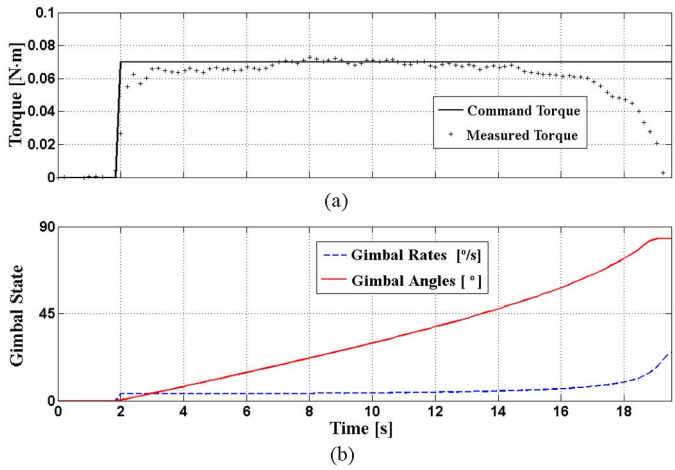

Fig. 18. Open-loop step response of the steering law: (a) Comparison of the desired torque to that measured. (b) Gimbal rate and gimbal excursion angles.

and no further torque can be generated in the desired direction. The gimbal rates determined by the steering law increase exponentially with gimbal excursion until they reach the limit of 25°/s imposed to prevent unreasonable gimbal rate commands near-singular orientations. Some losses are recorded beyond 50° excursion with rapid degeneration beyond 70°. These losses occur before the gimbal rate limit is reached and are due to the sampling frequency of the control system, which at 10 Hz becomes unable to keep up with rapidly changing gimbal rate commands. The results verify that the proposed steering law is exact and can be used in real-time applications. The errors described are due to the practical implementation of the steering law in a finite system. The limitations are not restrictive since the system is designed to meet its specification well within the boundary of its maximum momentum envelope.

B. Underwater Dynamics

The dynamics of the complete CMG, body, and fluid system are assessed using the underwater robot IKURA. The performance of the proposed control law is assessed by comparing

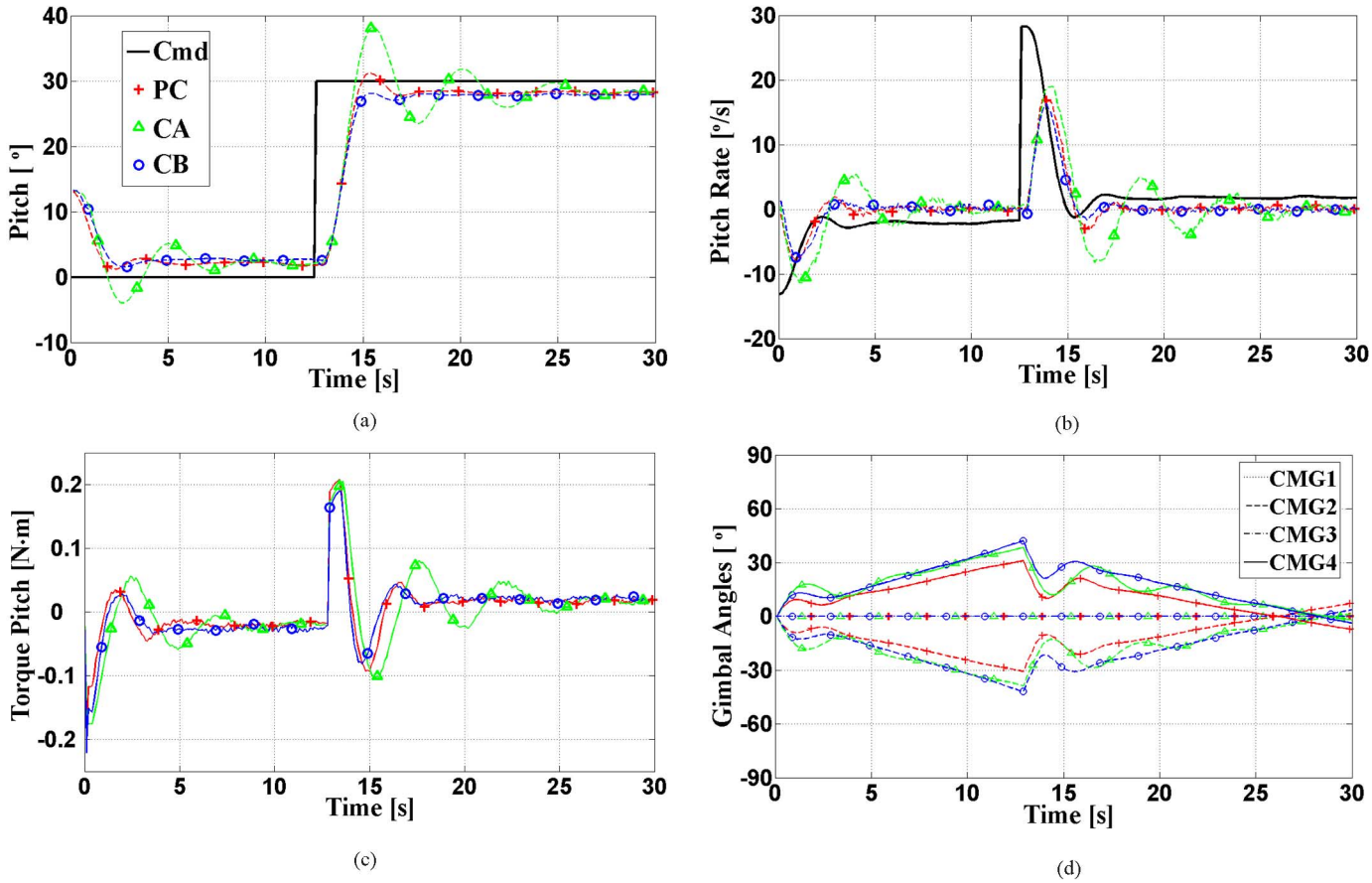

Fig. 19. Step response of the control system for $[k_q, k_w] = [0.5, 0.3]$: (a) and (b) pitch and pitch rate commands together with measurements obtained by the AHRS. (c) and (d) torque generated by the CMGs and the gimbal excursions. The proposed control law takes advantage of the coupled behavior of the CMG, body, and fluid system to achieve a superior response for less control activity than the alternative control laws. (a) Attitude. (b) Angular rate. (c) Torque. (d) Gimbal angle.

the closed-loop response of the robot to that with two alternative control laws. Next, an experiment is performed to verify the ability of the control system to actively stabilize the passively unstable, unsteady self-propelled translational dynamics of a Zero-G class underwater robot. This requires a fast response and a high resolution of attitude control and is essential for the practical application of Zero-G class underwater robots.

1) Control: The closed-loop response of the complete CMG, body, and fluid system is assessed in a series of underwater experiments using the proposed control law (PC) (14). To allow for comparison the experiments were repeated under identical conditions with two alternative control laws

$$\tau_{u_A} = \mathbf{Q}^T(\mathbf{q}) k_q \mathbf{e}_q + k_\omega \mathbf{e}_\omega$$
$$\tau_{u_B} = \mathbf{Q}^T(\mathbf{q}) k_q \mathbf{e}_q + [k_\omega \mathbf{e}_\omega - \mathbf{J}_{\text{tot}} \dot{\omega}_d - \omega \times \mathbf{\Pi}^* - u \times \mathbf{P}^*].$$

The first of these, control law A (CA), is a proportional–derivative controller that generates its command based only on the error in state. This control law is the feedback part of PC and neglects any feedforward modeling of the dynamics. The second, control law B (CB), also takes into account the dynamics of the CMG and body but, in contrast to PC, does not account for the hydrodynamic interactions of the body. The parameters $\mathbf{P}^*$ and $\mathbf{\Pi}^*$ are the linear and angular momentums (6) and (7) without the hydrodynamic terms $\mathbf{M}_A$ and $\mathbf{J}_A$.

Fig. 19 shows the response of the robot using the three different control laws with a flywheel rate of 8000 r/min. The robot first adopts a horizontal pitch angle and then a step pitch command of 30° is sent with the command pitch rate calculated as a function of the attitude error. The attitude and angular rate response [Fig. 19(a) and (b)] with CA is oscillatory and CB struggles to reach its final state. By modeling the coupled dynamics of the CMG and body, both PC and CB achieve a faster torque response [Fig. 19(c)] with an initial peak due to the derivative of the body rate command $\dot{\omega}_d$. The slower response of CA results in oscillations in the robot's attitude response. By modeling the hydrodynamic interactions of the body, PC generates larger torques than CB when the robot first accelerates and when it rotates at large rates to achieve a superior response by overcoming the hydrodynamic added inertia and viscous drag, respectively. This behavior results in significantly less control activity, with 30% smaller gimbal excursions than CB [Fig. 19(d)], making a more efficient use of the system. In each case, the robot's attitude falls short of the command with an offset of 3° using PC. Furthermore, the CMGs continue to exert a torque while the robot maintains its attitude. Since the experiments were carried out in a controlled environment with no currents or waves, the only explanation is that the robot has a small righting moment that works against the CMGs. This attitude offset can be overcome by including an integral error term in the control law.

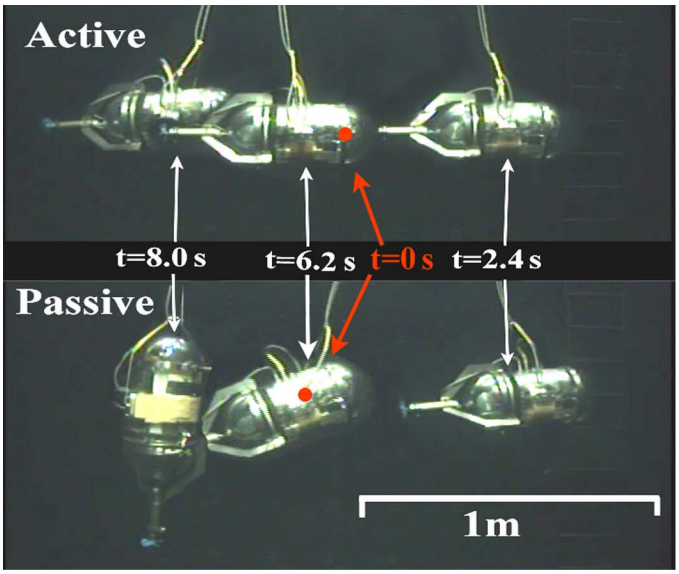

(a)

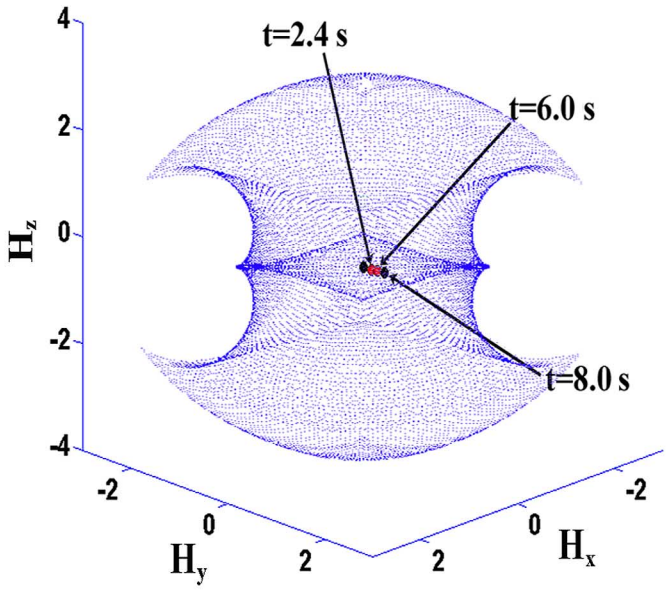

(b)

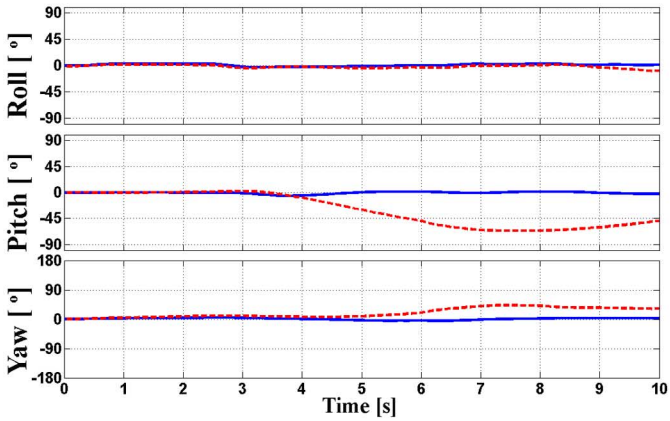

(c)

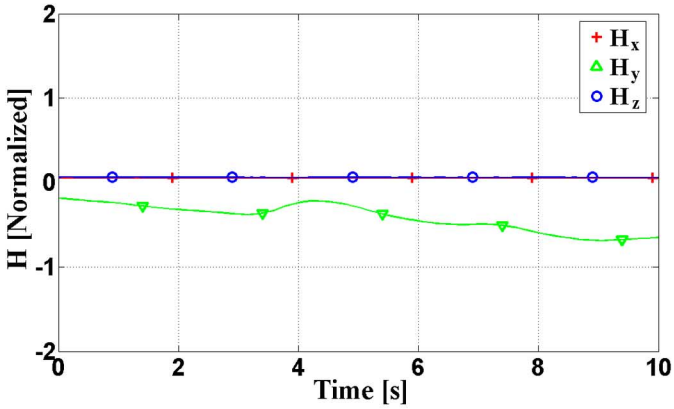

(d)

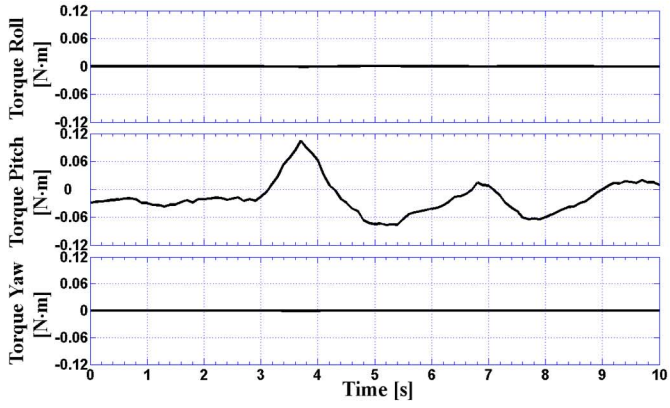

(e)

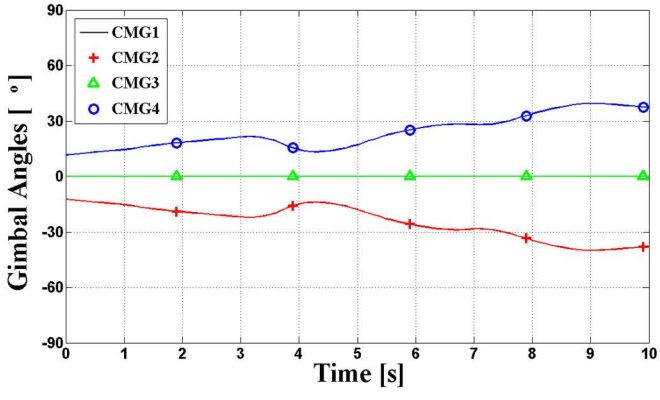

(f)

Fig. 20. Active stabilization of horizontal surge motion. (a) Comparison of the actively stabilized (top) and passive (bottom) response of the robot to identical thruster inputs. Any rotational effects of the safety cable are minimized by a hoop mechanism about the robot's longitudinal center. (b) Path taken by the CMG momentum vector in the constrained workspace in the active case. (c) Attitude of the robot measured by the AHRS unit. (d) Change in the CMG momentum vector to generate the torque in plot (e). (f) Gimbal excursions angles.

However, the CMGs would still have to resist the righting moment and would eventually reach the boundary of their operating envelope. A superior solution would be to eliminate or at least reduce the righting moment that forms the root of the problem.

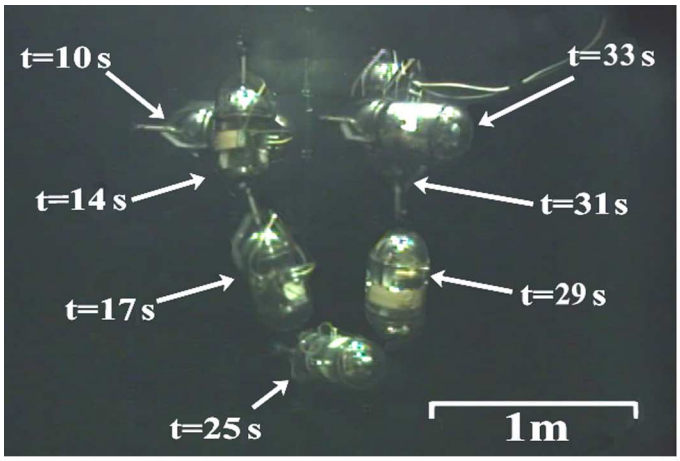

(a)

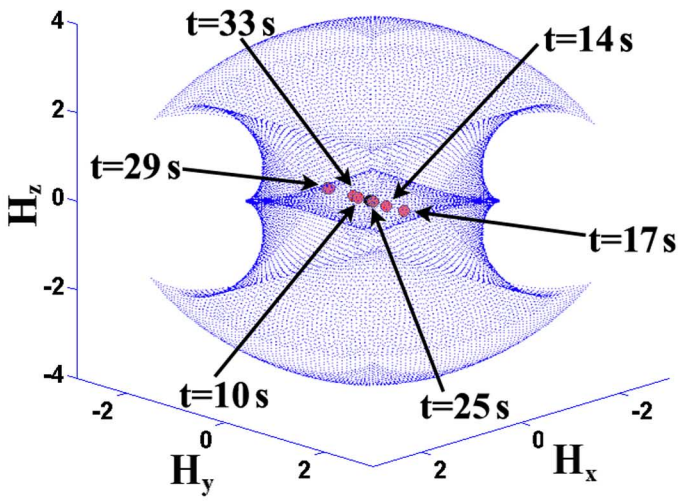

(b)

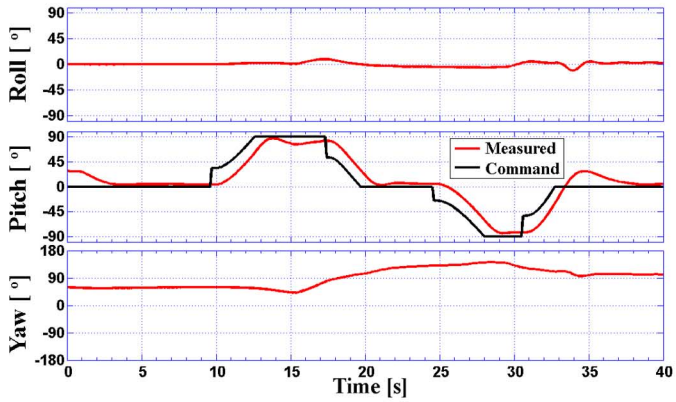

(c)

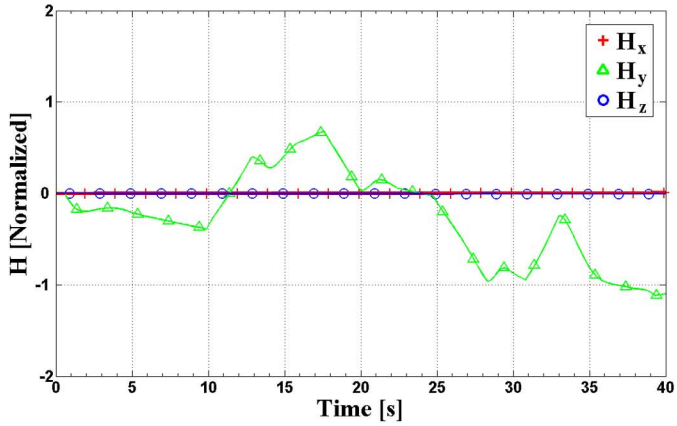

(d)

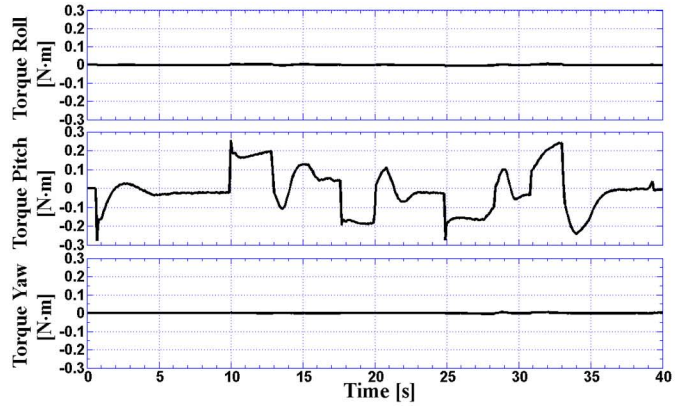

(e)

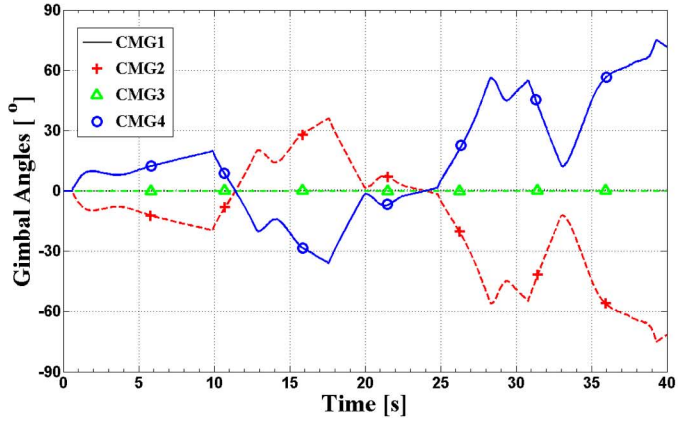

(f)

Fig. 21. Vertical pitched diving and surfacing in surge. (a) Image sequence taken by an underwater camera. (b) Path taken by the CMG momentum vector in the constrained workspace. (c) Control command and the attitude of the robot measured by the AHRS unit. (d) Change in the CMG momentum vector to generate the torque shown in plot (e). (f) Gimbal excursions angles.

2) Active Stabilization: Fig. 20 compares the actively stabilized and passive response of the robot during a horizontal surge maneuver. In the passive case, the flywheels are stationary and so the CMGs are inactive. In the active case, the flywheels rotate at 10 000 r/min and the CMGs respond to stabilize the robot's attitude. The image sequence in Fig. 20(a) shows that the active response to the back and forth maneuver is stable while the passive response is clearly unstable with the robot pitching more than

70° and yawing 45° [Fig. 20(c)]. In the active case, the CMG momentum vector moves along the y-axis [Fig. 20(b) and (d)] to generate torques in the order of 0.1 N·m, stabilizing the robot's attitude to within $\pm 3°$. The CMGs operates well within the constrained workspace [Fig. 20(b) and (f)]. The results verify that CMGs offer a sufficiently fast and high resolution of response to stabilize the passively unstable translational dynamics of the Zero-G prototype IKURA.

3) Summary: The actuation capabilities of the CMG system have been assessed in dry-land experiments to verify the CMG equations and demonstrate that the steering law developed is applicable in real time and remains exact to the desired torque. The performance of the control law has been assessed in underwater experiments, where despite the noncoincident centers of gravity and buoyancy, the proposed control law takes advantage of the coupled CMG, body, and fluid dynamics to achieve a superior control response for less overall control activity than two alternative control laws. Finally, the CMG system actively stabilized the passively unstable, unsteady self-propelled translational dynamics of a Zero-G class underwater robot, demonstrating a speed and resolution of control that is difficult to envisage being achieved using traditional actuators. The experiments establish that CMGs form an ideal basis for the attitude control system of Zero-G class AUVs.

X. Zero-G Maneuverability

This section demonstrates how a Zero-G class underwater robot can plan and optimize its missions in a 3-D manner, with the robot performing vertically pitched diving and surfacing in surge, as shown in Fig. 21. The image sequence in Fig. 21(a) shows the path followed by the robot. The robot first pitches to 90° with its nose down before diving vertically in surge. It then holds a horizontal attitude before pitching to −90° with its nose up to surface vertically. Finally, the robot rights itself to complete the maneuver. The CMG flywheels rotate at $\dot{\psi} = 10\,000$ r/min. Fig. 21(c) shows the attitude response of the robot during the experiment, where the CMGs exert a torque in the order of 0.2 N·m [Fig. 21(e)] during the pitching maneuver to adopt a vertical pitch angle. This is supported by Fig. 21(b) and (d) that shows the motion of the normalized CMG momentum vector to generate the required torques. Though the noncoincident centers of gravity and buoyancy place a significant demand on the CMGs, the momentum vector stays within the boundaries of the constrained workspace with the maximum gimbal excursions less than 90° [Fig. 21(f)]. The CMG system stores enough momentum at a flywheel rate of 10 000 r/min to exert the torques necessary to overcome the noncoincident centers of gravity and buoyancy of the robot used in this experiment, demonstrating a fast response and high resolution of control to actively stabilize the robot's attitude as it propels itself through the water in vertically pitched surge. This is, to the knowledge of the authors, the first time an underwater robot has performed vertically pitched diving and surfacing in surge. The results of this experiment verify that the proposed CMG attitude control system is capable of stabilizing any attitude on the surface of a sphere as the robot translates in surge and can provide Zero-G class underwater robots with unrestricted attitude control.

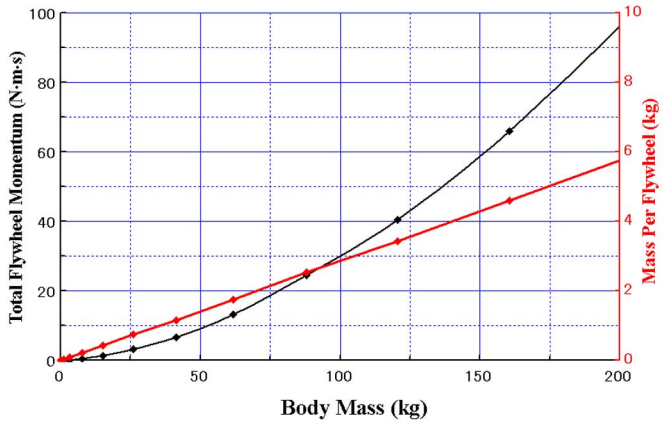

Fig. 22. Scaling of CMG momentum and mass with the size of the controlled body: The body has been modeled as a neutrally buoyant ellipsoid of revolution with uniform density and an aspect ratio of 2 : 1. The mass of the CMG flywheels has been calculated by scaling the flywheels used in IKURA to achieve the necessary angular momentum, as determined by an optimized bang–bang control law.

XI. Applications and Scaling

The freedom in attitude control offered by CMGs allows Zero-G class AUVs to plan and optimize their missions in a truly 3-D manner while travelling only in their principal mode of translation. Furthermore, the CMGs themselves are physically protected from the external environment and do not agitate fragile surfaces. The highly integrated design and high maneuverability at low speeds allow for maneuvering in confined spaces, making Zero-G class AUVs ideal for operation in geometrically complicated, cluttered, and even enclosed environments. Potential applications include tracking the dives of marine animals such as whales and turtles and extends to visual inspection and manipulation of man-made structures such as oil rigs, subsea oil wells, submerged ruins, and even the inside of pipes and sunken wrecks.

Fig. 22 illustrates how a CMG system would scale when applied to larger underwater robots. To maintain generality, the body of the robot has been modeled as a neutrally buoyant ellipsoid of revolution with constant density and an aspect ratio of 2 : 1, where the hydrodynamic properties have been calculated as detailed in [15], [25]. The mass of the CMG flywheels has been calculated by proportionally scaling the dimensions of the flywheels used in IKURA to achieve the necessary angular momentum, as determined by an optimized bang–bang control law. For similar controlled bodies, assuming the design and angular rate of the flywheels do not change, the mass of the flywheels necessary to meet the design specification of IKURA as given in Section VIII increases linearly with the mass of the controlled body.

While this paper has focused on the application of CMGs to Zero-G class AUVs, the theoretical and practical developments discussed are equally valid for smaller CMG systems that could be implemented on existing AUVs to stabilize roll and pitch motion for inspections or to provide a counteracting torque for manipulation tasks.

XII. Conclusion

The Zero-G has been designated as a new class of underwater robot that is capable of approaching its missions in a truly 3-D manner. A novel control scheme has been developed based on internal momentum exchange using CMGs that provides the necessary range and resolution of control about all three rotational degrees to allow Zero-G class underwater robots to adopt and maintain any attitude on the surface of a sphere with a zero radius turning circle and actively stabilize any attitude while translating in surge. The fully descriptive equations of motion of a CMG-actuated body moving through a fluid have been derived and the Lyapunov stability of a control law that models the coupled dynamics has been shown. A comprehensive geometric study has demonstrated why no exact, real-time steering law can guarantee singularity avoidance over the entire workspace of a minimally redundant CMG system. A global steering law that guarantees real-time singularity avoidance while maintaining exactness in a restricted workspace has been formulated based on the findings of the geometric analysis and the inverse kinematics of attitude control.

The CMG-actuated underwater robot IKURA is the first prototype Zero-G and is the first application of CMGs to underwater robots. A series of experiments has demonstrated the validity of the dynamic equations and the exactness of the real-time steering law. The experiments show that the control law developed takes advantage of the coupled dynamics of the CMG, body, and fluid system to achieve a superior response. Furthermore, the CMG system demonstrated the speed and resolution of control necessary to actively stabilize the robot's passively unstable translational dynamics. Unrestricted attitude control capabilities have been demonstrated and it is the first time an underwater robot has performed vertically pitched diving and surfacing in surge.

This research establishes CMGs as a new type of underwater actuator that offers a speed and resolution of response that is independent of the fluid environment and cannot be achieved using traditional actuation methods. The unrestricted attitude control and unique maneuvering capabilities demonstrated in this research allow Zero-G class underwater robots to plan and optimize their missions in a fully 3-D manner, taking advantage of their thrusters, sensors, and power supply in a way that has not been possible previously. This allows Zero-G class underwater robots to maneuver in confined spaces and so operate in geometrically complicated, cluttered, and even enclosed environments to perform missions that have so far eluded AUVs. The prototype Zero-G class underwater robot IKURA forms a unique platform with which to investigate potential applications and explore new fields of underwater research.

Acknowledgment

The authors would like to thank the Central Workshop of the Institute of Industrial Science, the University of Tokyo, and in particular T. Fukuo, for fabricating the components of IKURA.

References

[1] A. S. Brierley, P. G. Fernandes, M. A. Brandon, F. A. W. Millard, S. D. McPhail, D. Steven, P. Stevenson, M. Pebody, J. Perrett, M. Squires, D. Bone, and G. Griffiths, "Antarctic krill under sea ice: Elevated abundance in a narrow band just south of ice edge," *Science*, vol. 295, no. 5561, pp. 1890–1892, 2002.

[2] H. Iwakami, T. Ura, K. Asakawa, T. Fujii, Y. Nose, J. Kojima, Y. Shirasaki, T. Asai, S. Uchida, N. Higashi, and T. Fukuchi, "Approaching whales by autonomous underwater vehicle," *Mar. Technol. Soc. J.*, vol. 36, no. 1, pp. 80–85, 2002.

[3] K. Okamura, K. Yanai, Y. Sohrin, J. Ishibashi, M. Watanabe, and T. Ura, "In situ observations of dissolved manganese in hydrothermal vent plumes at Mariana Trough," *Eos. Trans. AGU*, vol. 85, no. 47, pp. V41B–1391, Dec. 2004, Fall Meeting Abstracts.

[4] B. A. A. P. Balasuriya, M. Takai, W. C. Lam, T. Ura, and Y. Kuroda, "Vision based autonomous underwater vehicle navigation: Underwater cable tracking," in *Proc. OCEANS*, 1997, vol. 1, pp. 1418–1424.

[5] H. Kondo, T. Maki, T. Ura, and T. Sakamaki, "Observation of breakwaters and their rock mound by AUV 'Tri-Dog 1' at Kamaishi Bay," in *Proc. IEEE OCEANS*, Brest, France, 2005, pp. 585–590.

[6] E. Yann, Y. Nose, and T. Ura, "Autonomous underwater sampling using a manipulator and stereovisual servoing," in *Proc. IEEE OCEANS*, Brest, France, 2005, vol. 2, pp. 731–736.

[7] K. Kawaguchi, T. Ura, Y. Tomoda, and H. Kobayashi, "Development and sea trials of a shuttle type AUV 'ALBAC'," in *Proc. 8th Int. Symp. Unmanned Untethered Submersible Technol.*, 1993, pp. 7–13.

[8] D. C. Webb and P. J. Simonetti, "The SLOCUM AUV: An environmentally propelled underwater glider," in *Proc. 11th Int. Symp. Unmanned Untethered Submersible Technol.*, 1999, pp. 75–85.

[9] N. Kato, "Control performance in the horizontal plane of a fish robot with mechanical pectoral fins," *IEEE J. Ocean. Eng.*, vol. 25, no. 1, pp. 121–129, Jan. 2000.

[10] K. A. McIsaac and J. P. Ostrowski, "Experimental verification of open-loop control for an underwater eel-like robot," *Int. J. Robot. Res.*, vol. 21, no. 10–11, pp. 849–859, 2002.

[11] N. E. Leonard and C. Woolsey, "Internal actuation for intelligent underwater vehicles," in *Proc. 10th Yale Workshop Adapt. Learn. Syst.*, New Haven, CT, 1998, pp. 295–300.

[12] C. Schultz and C. A. Woolsey, "An experimental platform for validating internal actuator control strategies," in *Proc. Guid. Control Underwater Veh. Conf.*, 2003, pp. 209–214.

[13] The Bendix Corp., "Control moment gyroscope gimbal actuator study," South Bend, IN, 1966, pp. 210–210.

[14] V. N. Branets, D. M. Weinberg, V. P. Verestchagin, N. N. Danilov-Nitusov, V. P. Legostaev, V. N. Platonov, P. S. Yu, V. S. Semyachkin, B. E. Chertok, and N. N. Sheremetyevsky, "Development experience of the attitude control system using single-axis control moment gyros for long-term orbiting space stations," in *Proc. 38th Congr. Int. Astronaut. Fed.*, 1987, pp. 8–8, IAF-87-04.

[15] F. M. White, *Fluid Mechanics*. New York: McGraw-Hill, 1979, pp. 700–700.

[16] J. E. Slotine and W. Li, *Applied Non-Linear Control*. Englewood Cliffs, NJ: Prentice-Hall, 1991, pp. 57–99.

[17] H. S. O. R. Vadali, "Feedback control and steering laws for spacecraft using single gimbal control moment gyros," *J. Astronaut. Sci.*, vol. 39, no. 2, pp. 183–203, 1994.

[18] NASA Marshall Space Flight Center (MSFC), "A comparison of CMG steering laws for high energy astronomy observatories (HEAOs)," Huntsville, AL, 1972, pp. 127–127.

[19] G. Margulies and J. N. Aubrun, "Geometric theory of single-gimbal control moment gyro system," *J. Astronaut. Sci.*, vol. 26, no. 2, pp. 159–191, 1978.

[20] E. N. Tokar and V. N. Platonov, "Singular surfaces in unsupported gyrodyne systems," *Cosmic Research*, vol. 16, no. 5, pp. 547–555, Mar. 1979.

[21] H. Kurokawa, "Constrained steering law of pyramid-type control moment gyros and ground tests," *J. Guid. Control. Dyn.*, vol. 20, no. 3, pp. 445–449, 1997.

[22] J. Paradiso, "A search based approach to steering single gimballed CMGs," NASA Johnson Space Center (JSC), Houston, TX, CSDL-R-2261, 1991.

[23] K. A. Ford and C. D. Hall, "Singular direction avoidance steering for control-moment gyros," *J. Guid. Control Dyn.*, vol. 23, no. 4, pp. 648–664, 2000.

[24] S. R. Vadali, H. S. Oh, and S. R. Walker, "Preferred gimbal angles for single gimbal control moment gyros," *J. Guid. Control Dyn.*, vol. 13, no. 6, pp. 1090–1095, 1990.

[25] F. H. Imlay, "The complete expressions for added mass of a rigid body moving in an ideal fluid," David Taylor Model Basin, Washington, D.C., Tech. Rep. DTMB, 1961.

Blair Thornton (M'07) received the B.Eng. degree in ship science and the Ph.D. degree in underwater robotics from the University of Southampton, Southampton, U.K., in 2002 and 2006, respectively.

He joined the Underwater Robotics and Application (URA) Laboratory, University of Tokyo, Tokyo, Japan, in 2003, where he spent three years as a Research Student and is currently a Postdoctoral Researcher. His research interests are underwater robotics and the development of Zero-G class AUVs.

Tamaki Ura (M'91–SM'02–F'07) graduated from the Faculty of Engineering, University of Tokyo, Tokyo, Japan, in 1972 and received the degree of Doctor of Engineering from the same university in 1977.

He founded the Underwater Robotics and Application (URA) Laboratory at the University of Tokyo, in 1978, and currently, he is the Director and Professor of the Underwater Technology Research Center at the Institute of Industrial Science (IIS), University of Tokyo. He is one of the leaders of AUV development in Japan, having constructed more than five ocean-going AUVs. Among these were the "R-One" robot that recorded 12-h continuous operation in 1998 and full autonomous exploration over Teisi Knoll in 2000. More recently, the AUV "r2D4" dived to a depth of 2700 m and discovered active hydrothermal vents in the midocean ridge system of the Indian Ocean using its onboard sensors. He coauthored *Underwater Robotics* (Tokyo, Japan: Seizando-Shoten, 1994), *Underwater Robotics* (Dordrecht, The Netherlands: Kluwer, 1996), and *Advances in Unmanned Marine Vehicles* (London, U.K.: Institution of Engineering and Technology, 2005, edited by Geoff Roberts and Robert Sutton, 2006).

Prof. Ura has been the Chairman of the IEEE Oceanic Engineering Society Tokyo Chapter since 1996. He has received three prizes from the Society of Naval Architects: the Paper Prize in 1979 and the Invention Prize in 1995 and 1997. He also received the Houku Prize in 1982 for significant contribution to the safety of moored ships, and the Prize of the High Automation Technology Association in 1998.

Yoshiaki Nose received the B.Sc. degree in physics from the University of Tokyo, Tokyo, Japan, in 1975.

He joined the Underwater Robotics and Application (URA) Laboratory, University of Tokyo, in 1978, as a Research Associate, where he has been actively involved in the development of more than five ocean-going AUVs and their operation. His research interests include both mechanical and electrical design of underwater robots.

Mr. Nose is a member of the Japan Society of Naval Architects and Ocean Engineers and the Japan Institute of Navigation.

Stephen Turnock received the B.A. degree in engineering from Pembroke College, University of Cambridge, Cambridge, U.K., in 1986, the M.S. degree in aeronautics and astronautics from the Massachusetts Institute of Technology (MIT), Cambridge, in 1988, and the Ph.D. degree on ship rudder–propeller interaction from the University of Southampton, Southampton, U.K., in 1993.

From 1986 to 1988, he was a Research Assistant at the Aeronautics and Astronautics Department, MIT. He joined then the Department of Ship Science, University of Southampton, in 1988, where he is now a Senior Lecturer at the School of Engineering Science. His research interests include computational fluid dynamics, AUV hydrodynamics and concept design, marine renewable energy, ship maneuvering, rudders, propulsion, and thrusters. He is the coauthor of a book on *Marine rudders and control surfaces* (London, U.K.: Butterworth, 2007).

Dr. Turnock is a member of the International Ship and Offshore Structures Specialist Committee V.4 Ocean wave and wind energy utilization, and is the Secretary of the 25th Information Technology Training Conference (ITTC) Propulsion Committee as well as an Editorial Board member of IMechE Part M: *Journal of Engineering in the Marine Environment*.